Summer 1997

Damage detection of bridge-like structures using state space models

Javier Valentin Sivico

Department:

DAMAGE DETECTION OF BRIDGE-LIKE STRUCTURES

USING STATE SPACE MODELS

by

JAVIER VALENTIN SIVICO, 1972 -

A THESIS

Presented to the Faculty of the Graduate School of the

UNIVERSITY OF MISSOURI - ROLLA

In the Partial Fulfillment of the Requirements for the Degree

MASTER OF SCIENCE IN ELECTRICAL ENGINEERING

1997

Approved by

Dr. Vittal S. Rao, Advisor

Dr. Kelvin T. Erickson

Dr. K. Chandrashekhara

ABSTRACT

A global damage detection algorithm for bridge-like structures is proposed. This method provides the capability of determining the reduction in both stiffness and damping parameters of the structural elements. It is assumed the mass of the structural elements is not affected by the damages, which is a reasonable assumption for bridge-like structures. The proposed method uses the state space representation of the structural dynamics to make the diagnosis of the structural integrity. Given that the state space representation of any system is not unique, the damage detection procedure is developed for the physical coordinates of the state space representation. A transformation method to get any arbitrary state space representation into the physical coordinates is also developed.

The feasibility of the proposed damage detection algorithm is verified on a numerical example as well as on a simulated three-bar truss structure with three degrees-of-freedom.

ACKNOWLEDGEMENT

Thanks God for your love, mercy and strength. Millie, thank you for your love, support, encouragement and patience; and for bringing our beloved and precious baby, Angel Javier Valentín Rodríguez, to this world. I love you both; part of this degree belongs to you. Thanks to my family and relatives who had always encouraged and supported me. I will like to thank the Presbyterian Church at Esteves (Aguadilla, Puerto Rico) and to the First Presbyterian Church of Rolla for your care and prayers; also to the Presbyterian Church (U.S.A.) for your financial support through the Presbyterian Church Student Opportunity Fellowship during my undergraduate studies at the University of Puerto Rico, Mayagüez Campus. I will also like to thank the Johns Hopkins University Applied Physics Laboratory and the GEM Fellowship for your financial support through my graduate studies. The support of the Mid-America Transportation Center is also acknowledged.

Thanks to Dr. Vittal S. Rao, Dr. Kelvin T. Erickson and Dr. K. Chandrashekhara for serving on my graduate committee; and to the Smart Structure Group for your technical and non technical support.

Finally, thanks to all those people who in one way or other had helped me to be who I am today. To all of you, GRACIAS!

TABLE OF CONTENTS

Page

LIST OF ILLUSTRATIONS

Figures Page

LIST OF TABLES

I. INTRODUCTION

Even when structures are carefully designed for load carrying capabilities, they may be prone to damage during their service life. Undetected damage may grow to the point where it may cause catastrophic failure in which many lives may be lost. In order to assure the integrity of a structure, it should be submitted to periodical inspection. Inspecting large structures requires lot of time and qualified personnel; making inspection a very expensive and time consuming procedure. Additionally, there are faults which are impossible to detect with the naked eye because they are at the center of the structural elements, or because the inspector does not have access to that particular structural region. These are some of the reasons why in recent years, a considerably amount of effort had been put into the research and development of damage detection algorithms (DDA) for structures.

Due to the interest in aerospace studies and the development of a space station, a lot of attention has been given to the space structures which, in general, are lightly damped. For this reason, most of the global damage detection algorithms (GDDA) developed for these kind of structures do not address the damping reduction of the structural elements. By other hand, in bridge-like structures the damping of the structural elements constitutes a very important factor of the structural response. This is why a GDDA for bridge-like structures should address the damping reduction of the structural elements. Another characteristic of the bridge-like structures is that damage does not considerably affect the mass of the damaged structural element.

The presence of damage in a structure causes it to behave different to its healthy counterpart. As the structure accumulates damage, certain structural characteristics, such

as natural frequencies and mode shapes, change. These changes are the consequence of changes in structural parameters such as mass, stiffness and damping.

A GDDA should not only be able to determine that a structure has been damaged, but it should also determine which structural elements have been damaged and the damage severity. In order to make a diagnosis of the structural integrity, a GDDA requires knowledge of the structural response to external forces; the structural response can be observed in either time domain or in the frequency domain. A GDDA based on the time domain provides for on-line application of the algorithm; while a GDDA based on frequency domain data can only be applied off-line. Having a method which can be applied on-line avoids the deadtime of the structure; in other words, the structural integrity can be tested while the structure is kept on its regular use.

A model of the structure is required in order to detect and classify the damages in the structure. The finite element method for truss structures with bar elements will be reviewed. In addition, two techniques for obtaining a state space representation of the structure from its structural response will also be reviewed. The first of these procedures generates a state space representation based on the sweep sine frequency response of the structure. The second system identification is the Eigensystem Realization Algorithm, in which a discrete time state space representation is obtained using the Markov parameters of the structures. In order to estimate the structural Markov parameters, a neural network based procedure is reviewed.

A GDDA for bridge-like structures is proposed in this thesis. The proposed algorithm provides for determining stiffness and/or damping reduction of the structural elements, while assuming that their mass does not vary due to damage. This GDDA is

based on the state space representation of the structure, which is identified from time domain data. Considering that the state space representation for a system is not unique, this method has been developed using the state space representation corresponding to the physical coordinates of the structure. The state space representation of a structure determined using an appropriate system identification method contains an arbitrary set of states. Therefore, a linear transformation is required to transform the identified arbitrary state space representation into the structural physical coordinate. A method to determine this linear transformation is also proposed. In order to validate the proposed GDDA, it has been applied on a numerical example as well as on a simulated three-bar-truss structure with three degrees-of-freedom (DOF).

II. LITERATURE SURVEY

In recent years, the smart structure community has been interested in the research and development of algorithms for damage detection in structures. Safety and inspection costs are the two main reasons for this special interest. In addition, the development of a space station has greatly contributed to the development of damage detection algorithms (DDA). The objective of a DDA is not only to indicate when a structure has been damaged; in addition, it should also indicate which section or element has been damaged, what kind of damage has occurred and the extent of the damage.

Based on what kind of damage a particular DDA identifies and what kind of data it uses, it may be classified into several classes of algorithms. Some algorithms are classified as global damage detection algorithms. The objective of a global damage detection algorithm (GDDA) is to verify the integrity of a whole structure, and narrow down the inspection problem to specific regions or elements. Once a particular region has been identified as damaged, local DDA can be applied for further investigation of the fault. Some DDA are based on the frequency response of the structure, while others are based on the time domain response. Algorithms based on time domain data are suitable for real time damage detection; while algorithms based on frequency domain response may be applied off-line.

Every DDA requires information about the structural response to external forces. A common approach for damage detection is to compare a mathematical model of the damaged structure versus the mathematical model of the healthy structure. The mathematical model for the damaged structure is usually obtained

from the structural response, while a mathematical model for the healthy structure comes for the finite element model (FEM). Other GDDA have been developed using artificial intelligence technology, such as pattern recognition and neural networks; several GDDAs of these categories will be reviewed.

The global DDA proposed in this thesis identifies, classifies and estimates the structural damage by comparing the physical coordinate state space model of the damaged structure versus the corresponding state space model of the healthy structure. Also, two other methods with similar approaches will be discussed in detail. These methods are the Best Achievable Eigenvector method and the method proposed by Chen and Garba. In addition to the reviewed GDDAs, one local DDA will be reviewed. This algorithm identifies faults by monitoring the local electrical impedance using piezoelectric patches.

A. DAMAGE DETECTION USING MODAL RESPONSE

In recent years, many researchers[1,2,3,4] have investigated the use of the structural modal response for the assessment of the structural integrity. Due to the development of a space station, most of this effort has been dedicated to the damage detection for space structures, which in general, are lightly damped. Therefore, many of the developed DDA address the reduction in stiffness and/or mass of the structural elements neglecting their damping.

Every DDA based on the structural modal response requires information on the structural response to external forces, structural identification and some method to compare the obtained structural model to the model for the healthy structure. Smith et al.[3], describes the general steps involved in any DDA which uses modal test for

damage assessment; these steps are summarized in Figure 1. In Figure 1, each solid vertical line represents a process which may be performed by different algorithms. In this figure, modal data refers to natural frequencies and mode shapes, which are obtained using a model identification algorithm. For space structures, the original model usually consist of the global mass and stiffness matrices; for other structures, the damping matrix may also be required. Some DDA may require normalized mode shapes. Very often, measurements are made at only a few degrees-of-freedom (DOF), necessitating expansion of the identified mode shapes[5].

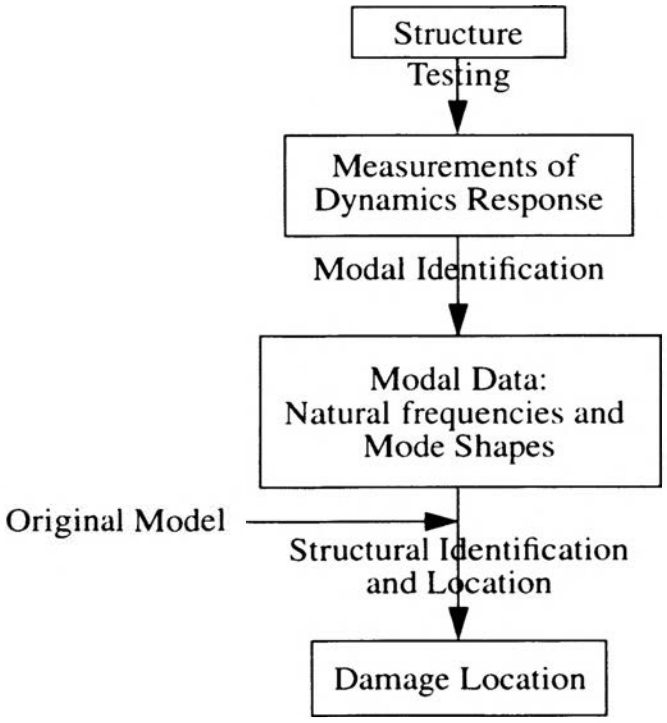

Figure 1. Steps for a DDA using structural modal response

Several sets of algorithms may be chosen to perform the steps shown in Figure 1. Smith presented the obtained results using one particular set of algorithms applied to an 8-bay truss structure. The importance of preserving the load path during the structural identification is emphasized. An iterative stiffness matrix identification algorithm was used for structure identification purpose. This algorithm produces a minimally changed model to match the modal data while preserving the load paths of the original structure. A method that uses graph theory for a matrix was used for damage location[4]. The zero-nonzero pattern of a matrix is represented by a graph for that matrix. The node and the percentage of edge adjustment are stored in two vectors, producing two lists. One list represents the adjustment to the elements of the diagonal, while the other represents the adjustment to the non-zero elements of the off-diagonal. These two lists are filtered with two threshold values for damage detection, resulting on a subgraph for the damaged structure. The resulting subgraph indicates the damaged structural elements.

In the next two sections, two methods for damage detection which use modal response will be reviewed in details. These two DDAs are the Chen and Garba method and the Best Achievable Eigenvector technique.

1. Method by Chen and Garba The Chen and Garba method[1] assumes that the structure does not contain any damping. Additionally, it assumes that the mass distribution of the structure is not affected by the damage, or that it changes by a known quantity. This method only provides for changes in the stiffness parameters.

The existence of damage is determined by a relatively large change in natural frequencies and mode shapes. The authors show that the kinetic energy distribution

at each DOF for each mode is equal to the potential energy distribution for that particular mode:

$$\underbrace{[\phi]_i^d [K]\{\phi\}_i}_{\text{Potential Energy}} = \underbrace{\omega_i^2 \left\{ M_{jj}\phi_{ji}^2 \right\}}_{\text{Kinetic Energy}} \tag{1}$$

where $\{\phi\}_i$ is the mode shape associated to the i^{th} mode, ω_i is the i^{th} mode natural frequency, $[\ ]^d$ represents a diagonal matrix, and j refers to the j^{th} position of the vector or matrix. Note that the kinetic energy distribution can be calculated using the measured natural frequencies, ω_i, and measured mode shapes, ϕ_i. The potential energy distribution of the DOF associated with a damaged structural element will be different from its undamaged counterpart. Considering this, the locations of the damage are determined by finding the DOFs for which the kinetic energies are different from their values for the healthy structure.

In order to determine the extent of the damage, the connectivity matrix for each mode is used. The connectivity matrix is determined by expanding the expression $[\Delta k_{ij}]\{\phi\}_i$ (where the matrix $[\Delta k_{ij}]$ is determined from the finite element model of the structure), and expressing it as $[C]_i\{\Delta k_{ij}\}$. Finally, the extent of the damage, Δk_{ij}, is determined by solving a constrained minimization problem of the stiffness change norm.

The governing equation for the structural dynamics can be written as

$$[M]\{\ddot{x}\} + [C]\{\dot{x}\} + [K]\{x\} = \{f(t)\}. \tag{2}$$

Given that the space structures are lightly damped, the damping matrix $[C]$ will be zero, or very close to zero. Therefore, the corresponding homogenous equation for Equation (2), for a lightly damped structure may be formulated

$$[M]\{\ddot{x}\} + [K]\{x\} = 0 \quad . \tag{3}$$

This global damage detection algorithm (GDDA) assumes that the mass distribution of the structure, matrix $[M]$, is not affected by a damage, or that it changes by a known quantity. The solution for the differential equation, Equation (3), can be expressed as

$$\{x\} = \{\phi\}_i \sin\omega_i t \, . \tag{4}$$

Substituting the solution to Equation (3) as expressed in Equation (4), the following relationship is obtained:

$$[K]\{\phi\}_i - \omega_i^2 [M]\{\phi\}_i = 0 \, . \tag{5}$$

From Equation (5) it can be seen that any mass and/or stiffness loss will be reflected in the structural natural frequencies and mode shapes. Therefore, a deviation from the original natural frequencies and mode shapes will indicate damage occurrance. Note that changes in some physical parameters will affect some structural modes, and not necessarily all the structural modes. Pre-multiplying Equation (5) by a diagonal matrix, $[\phi]_i^d$, which contains the i^{th} mode shape as its diagonal, and considering the matrix $[M]$ to be diagonal (lumped mass matrix),

$$[\phi]_i^d [K]\{\phi\}_i = \omega_i^2 [\phi]_i^d [M]^d \{\phi\}_i = \omega_i^2 \left\{ M_{jj} \phi_{ji}^2 \right\} . \tag{6}$$

The left hand side of Equation (6) represents potential energy distribution, while the right hand side represents kinetic energy distribution. Therefore, Equation (6) shows that the kinetic energy distribution for the i^{th} mode is equal to its potential energy. Note that the kinetic energy for the i^{th} mode can be computed once the natural frequency, ω_i, and the mode shape, $\{\phi\}_i$, had been determined from the measured vibration response of the structure. The location of the damage can be found by identifying kinetic energy values of DOF which are different from the healthy structure.

Once a structure has been damaged, its stiffness matrix can be expressed as

$$[K] = [K_0] + [\Delta K], \tag{7}$$

where the delta matrix, $[\Delta K]$, is due to the damage; and it contains variables for the stiffness variations of the structural elements. Substituting Equation (7) in Equation (5),

$$[\Delta K]\{\phi\}_i = (\omega_i^2[M] - [K_0])\{\phi\}_i. \tag{8}$$

The left hand side of Equation (8) can be manipulated, in such a way that

$$[\Delta K]\{\phi\}_i = [C]_i\{\Delta k_{ij}\}, \tag{9}$$

where $[C]_i$ is referred as the connectivity matrix for the i^{th} mode. Substituting Equation (9) in Equation (8),

$$[C]_i\{\Delta k_{ij}\} = \{y\}_i \tag{10}$$

where

$$\{y\}_i = (\omega_i^2[M] - [K_0])\{\phi\}_i. \tag{11}$$

Note that $\{y\}_i$ is know for all the pairs of natural frequencies, ω_i, and mode shape, $\{\phi\}_i$. Equation (10) can be augmented for N modes, so that,

$$\begin{bmatrix} [C]_1 \\ \cdots \\ [C]_N \end{bmatrix}_{N \times M} \{\Delta k_{ij}\}_{M \times 1} = \begin{Bmatrix} \{y\}_1 \\ \cdots \\ \{y\}_n \end{Bmatrix}_{N \times 1}, \tag{12}$$

where N is the number of equations, and M is the number of stiffness variations Δk_{ij}. In order to solve for Δk_{ij}, the pseudo-inverse should be used for all the three possible cases:

$M > N$:

$$\{\Delta k_{ij}\} = [C]^T([C][C]^T)^{-1}\{Y\} \tag{13}$$

$M < N$:

$$\{\Delta k_{ij}\} = ([C]^T[C])^{-1}[C]^T\{Y\} \tag{14}$$

$M = N$:

$$\{\Delta k_{ij}\} = [C]^{-1}\{Y\}\text{`}. \tag{15}$$

2. Best Achievable Eigenvector Method The Best Achievable Eigenvector (BAE) method[2] also assumes no damping in the structure, and considers the damage to be a reduction in stiffness and/or mass. It also assumes the mode shapes at the finite element degrees-of-freedom (DOF) are available either by expanding the mode shapes at the test DOF or by measuring the entire finite element DOF.

In this study, the situation of insufficient mode shapes is not addressed. In this method, possible damage locations are identified using the BAE concept. The BAEs

are defined by the undamaged analytical model and the measured natural frequencies. The Euclidean distance between the BAEs and the measured mode shapes are used to determine possible damage locations. Once the possible damaged structural elements have been identified, the extent of the damage is determined using constrained eigenstructure assignment. In the case of multiple damage and/or multiple possible damage locations, an iterative procedure is suggested.

The equation of motion for an n-DOF structural dynamic system without damping can be expressed as

$$M\ddot{x} + Kx = f(t) \tag{16}$$

The eigenvalue equation associated with equation (16) is

$$K\Phi = M\Phi\Lambda \tag{17}$$

where: Φ is an $n \times r$ system modal matrix, and Λ is a diagonal matrix containing the n eigenvalues. Each structural element contributes to the overall system mass and stiffness, M and K respectively; so that these matrices can be expressed as the summation of each structural element contribution, i.e.

$$K = \sum_{i=1}^{p} K_i, \tag{18}$$

and

$$M = \sum_{i=1}^{q} M_i. \tag{19}$$

Once a structural member is damaged, its stiffness and/or damping parameter is reduced by a certain percent, which are called reduction factors. Therefore, the structural matrices for a damaged structure can be expressed as

$$K_d = K_u + \sum_{i=1}^{p} a_i K_i \tag{20}$$

and

$$M_d = M_u + \sum_{i=1}^{q} b_i M_i, \tag{21}$$

where the subscript d refers to the damaged structure, a_i is the stiffness reduction factor for the i^{th} structural member and b_i is the mass reduction factor for the i^{th} structural member. The reduction factors a_i and b_i can take any value in the range $[-1,0]$. The reduction factor vector, s, is defined to be

$$s = \begin{bmatrix} s_1 \\ \cdots \\ s_p \\ s_{p+1} \\ \cdots \\ s_{p+q} \end{bmatrix} = \begin{bmatrix} a_1 \\ \cdots \\ a_p \\ b_1 \\ \cdots \\ b_q \end{bmatrix}. \tag{22}$$

Considering the expressions for the matrices K_d and M_d as given in Equations (20) and (21), together with r number of tested modes, the eigenvalue equation, can be re-arranged as

$$\sum_{i=1}^{p} a_i K_i \Phi_t - \sum_{i=1}^{q} b_i M_i \Phi_t \Lambda_t = M_u \Phi_t \Lambda_t - K_u \Phi_t, \tag{23}$$

where the subscript t denotes a tested quantity. With the following definitions,

$$E_j = \omega_{tj}^2 M_u - K_u \tag{24}$$

$$A_{ij} = E_j^{-1} K_i \tag{25}$$

and

$$B_{ij} = -\omega_{tj}^2 E_j^{-1} M_i, \tag{26}$$

Equation (23) can be expressed as

$$\sum_{i=1}^{p} a_i A_{ij} \phi_{tj} + \sum_{i=1}^{q} b_i B_{ij} \phi_{tj} = \phi_{tj}. \tag{27}$$

Assuming there is only one structural member damaged, say element k, and that it only affects the j^{th} mode, it is desired to verify the influence of the reduction factor s_k on the j^{th} mode. With this single damage scenario, it will be found that the element d_{kj} of the matrix D,

$$D = \begin{bmatrix} d_{11} & \cdots & d_{1j} & \cdots & d_{1r} \\ \cdots & \cdots & \cdots & \cdots & \cdots \\ d_{k1} & \cdots & d_{kj} & \cdots & d_{kr} \\ \cdots & \cdots & \cdots & \cdots & \cdots \\ d_{e1} & \cdots & d_{ej} & \cdots & d_{er} \end{bmatrix}, \tag{28}$$

will be zero or very close to zero. In the definition of matrix D, e is the number of structural elements that could possibly have caused the damage, and d_{kj} is the Euclidean distance between the measured modes and the best achievable eigenvector (BAE) defined by the undamaged analytical model and the measured natural frequencies; so that,

$$d_{kj} = \left\| \phi_{tj} - \phi_{kj}^a \right\|, \tag{29}$$

where

$$\phi_{kj}^a = \hat{L}_{kj} \hat{L}_{kj}^{\dagger} \phi_{tj}. \tag{30}$$

In equation (30), $\hat{L}_{kj}$ is the matrix L_{kj} without the zero columns; and L_{kj} is defined to be,

$$L_{kj} = \begin{cases} A_{kj}, k = 1, \ldots, p \\ B_{(k-p)j}, k = p+1, \ldots, p+q \end{cases} . \tag{31}$$

This method for determining which structural element has been damaged, is based on the fact that, if the damage has been caused by the stiffness or mass loss of element k, and this damage is reflected in the j^{th} mode, then the measured mode shape must be a linear combination of the columns of the matrix L_{kj}. In other words, the measured mode ϕ_{tj} must reside on the span of the matrix L_{kj} column vectors.

Once the matrix D is determined, different possible damaged members are identified by verifying which elements of the matrix D are zero or very close to zero. Using these possible damaged members, $\hat{p}$ number of stiffness elements and $\hat{q}$ number of mass elements, equation (27) can be re-written as

$$\sum_{i=1}^{\hat{p}} a_i \hat{A}_i + \sum_{i=1}^{\hat{q}} b_i \hat{B}_i = R, \tag{32}$$

where

$$\hat{A}_i = K_i \Phi_t, \tag{33}$$

$$\hat{B}_i = -M_i \Phi_t \Lambda_t \tag{34}$$

and

$$R = M_u \Phi_t \Lambda_t - K_u \Phi_t . \tag{35}$$

Equating each column of equation (32), and re-arranging the obtained equation,

$$\hat{L}\hat{s} = r \tag{36}$$

where

$$\hat{s} = \left[a_1 \ \cdots \ a_{\hat{p}} \ b_1 \ \cdots \ b_{\hat{q}}\right]^T, \tag{37}$$

$$\hat{L} = \begin{bmatrix} \hat{A}_{11} \ \cdots \ \hat{A}_{\hat{p}1} \ \hat{B}_{11} \ \cdots \ \hat{B}_{\hat{q}1} \\ \hat{A}_{12} \ \cdots \ \hat{A}_{\hat{p}2} \ \hat{B}_{12} \ \cdots \ \hat{B}_{\hat{q}2} \\ \cdots \ \cdots \ \cdots \ \cdots \ \cdots \ \cdots \\ \hat{A}_{1r} \ \cdots \ \hat{A}_{\hat{p}r} \ \hat{B}_{1r} \ \cdots \ \hat{B}_{\hat{q}r} \end{bmatrix} \tag{38}$$

and

$$r = \left[R_1^T \ \cdots \ R_r^T\right]^T; \tag{39}$$

where $\hat{A}_{ij}$ and $\hat{B}_{ij}$ represent the j^{th} column of the matrices $\hat{A}_i$ and $\hat{B}_i$, respectively, and R_j is the j^{th} column of the matrix R. The reduction factor vector, $\hat{s}$, can be solved from equation (36),

$$\hat{s} = \hat{L}^{\dagger} r, \tag{40}$$

where $\hat{L}^{\dagger}$ is the pseudo-inverse of $\hat{L}$.

If there are multiple possible damaged elements, an iterative process is suggested:

Step 1: the single must probable damage member is selected examining matrix D.

Step 2: the reduction factor, $\hat{s}$, for that member is determined using Equation (36).

Step 3: a "new undamaged" stiffness or mass matrix is computed considering the reduction factor computed in Step 2. For example: $K_u' = K_u + \hat{s}_k K_k$.

Step 4: compute the natural frequencies using the "new undamaged" matrix from Step 3.

Step 5: if the natural frequencies are very close to the measured ones, then all the damaged elements had been properly identified; if not, a new matrix D is computed, and the process is repeated.

From the discussed procedure, it can be seen that the BAE involves two sub-procedures, the first one to determine which structural elements have been damaged, and a second one to determine the respective reduction factor.

B. NEURAL NETWORKS FOR STRUCTURAL DAMAGE DETECTION

Many researchers[6,7,8,9,10] have investigated the application of neural networks to the structural damage detection problem. Most of the studies follow the same idea or procedure: a measurable mechanical property is identified as the network input, and the location(s) and/or extent of the damage as the output of the network. The network architecture is varied until one is found which is able to learn the input-output relationship. Then, the network is tested with some cases for which the network was not trained; this is to determine the quality of the generalization achieved by the trained network. Consider three different studies in which neural networks have been applied for damage detection.

1. Neural Networks for Damage Detection in a Three Story Building Wu et al.[10], considered a study in which a neural network is used to identify the damage location

and its extent in a simulated-three story building. In this study, the columns of each story were considered to be a structural element; and the damage was modeled as a reduction in the stiffness of one of the structural elements, ignoring their damping. The building was excited at the base using data from several earthquakes. The acceleration at the top floor was Fourier transformed and discretized into 200 intervals (in the range of 0 - 20 Hz). This discretized Fourier-transformed data constituted the input to the network. The training data set consisted of the no-damage case, 50% and 70% reduction of stiffness for each of the three structural elements (only one at a time); and each of these cases for six different earthquakes, for a total of 42 different damage cases. A network architecture that learned the training set included the following: input layer of 200 nodes, one hidden layer of 10 nodes, and the output layer of three nodes. The value at the output nodes represent the stiffness percent still present at the structural element. When the network was tested with the untrained-for case of 60% reduction in each of the three structural elements (one at a time), it was found that the network only identified properly the damage at the third floor. This level of generalization is unacceptable. Therefore, the authors proceeded to add an extra accelerometer at the second floor. This forced a modification of the architecture, which was modified to have two input sets of 200 nodes each, two hidden layers and an output layer with 3 nodes. After training the network, and testing it with the untrained-for case of 60% stiffness reduction at each of the structural elements (one at a time), it was found that the network was able to identify the location and extent of the damage at the third and first floors. It was still unable to identify properly the damage at the second floor.

This particular study demonstrated that a neural network could be used for damage detection, but many questions remain on the table, such as: how much information will the network need in order to learn the training cases? From which locations should this information come? How many damage cases should the network learn before reaching an accurate level of generalization? These questions are in addition to the still unsolved enigma of determining a network that will learn a particular input-output relationship. Additionally, it should be noted, that the untrained-for case that was considered in this paper was in the range for which the network was trained. If it was not on that particular range, the level of generalization may not be applicable.

2. Neural Networks for Damage Detection in Mass-Damper-Spring Systems Tsou and Shen[8] used different neural networks to detect reduction in the stiffness of the springs in two different systems. The first considered system was a mass-damper-spring system with 3-DOF, while the second one was an mass-spring system with 8-DOF which had closely-spaced natural frequencies. For the 3-DOF system, a three layer backpropagation neural network was able to identify single spring damages within 3.5 relative percentage error if the stiffness reduction was within the range considered during the network training, which was from 10 to 90 percent reduction with intervals of 10 percents. The input of the neural network were the changes in the natural frequencies once the damage was considered; and the output of the network represented the stiffness of the three springs. For the cases of multiple damages, a three layer backpropagation neural network was also used for damage

detection purpose. The obtained results using the trained network were also excellent; the identified damage was within 5.5% the actual stiffness variation.

For the considered 8-DOF system, which had closely-spaced natural frequencies, the required neural network architecture was very complex. For this problem, the neural architecture was divided into three sub-networks. The first sub-network consisted of a single layer which had the 8-DOF modal data as inputs, and the weights were the elements of the system mass and stiffness matrices. The resulting output vector was a signed vector, d_i, which represented a transformed eigenvector. This vector, d_i, was the input to the second sub-network; which had three layers and was pre-trained to identify which of the 14 springs had their stiffness parameter reduced. Finally, the third sub-network had the output of both first and second sub-networks as it inputs. The output of the last sub-network represented the estimation of the damages. This network was able to identify the considered multiple damages within 3.2% of the actual damage if the stiffness reduction were in the range used during training. If the reduction was out of this range, a maximum of 35% error was experienced.

The obtained results indicate the feasibility of using neural networks for damage detection. And the need for a wide range of damage cases during the network training was demonstrated.

3. Vibration Signature Analysis Using Artificial Neural Networks The questions of number of sensors and optimal sensor placement were addressed by Barai[6]. In this work, the results of using a multilayered neural network for the identification of stiffness reduction on a simulated bridge-like planar truss structure with 21-DOF

were presented. The training data was obtained by simulating the FEM of the structure under different damages scenarios. The damages were considered to be a reduction of stiffness, which were modeled as reduction in the structural elements cross-sectional area. The external forces were considered to be the effect of a single load moving along the bridge at a constant speed. The moving forces were converted into stationary time dependent forces. On simulation, the amount of available vertical displacement sensors was considered to be 1, 3 and 5. The simulated measurements were normalized to have values between 0 and 1; the normalization was done to improve the convergence during training.

The neural network architecture that learned the training set had 4 layers of neurons: the input layer, 2 hidden layers and the output layer. The two hidden layers had 21 neurons each. The output layer had 21 neurons corresponding to the cross-sectional area of the respective 21 structural elements. The number of neurons at the input layer varied depending on how many vertical displacement sensors were considered. For the cases with one, three and five sensors the input layer respectively had 69, 72 and 74 neurons; 69 neurons received the vibration signature data and the other inputs were used to code which sensor the data was coming from.

After training the neural network with 16 different damage scenarios, the generalization of the network was tested using 5 cases not included on the training set. It was found that the best damage detection was achieved considering only one sensor, placed on a suitable location. The single sensor was considered to be at different DOF, but the best results were obtained with the single sensor placed at the vertical DOF at the center of the bridge span, at the bottom of the structure.

The fact that the network was able to properly identify the location and extent of the damage considering only one single sensor was the main result of this work. The high level of structural symmetry together with a noise-free environment may had contributed to the obtained results.

C. DAMAGE DETECTION USING PATTERN RECOGNITION

Tang et al.[11], presents how the statistical approach of pattern recognition could be used for damage detection on a composite beam. As shown in Figure 2, using the statistical approach of pattern recognition for damage detection involves four general steps: pattern measurements, feature extraction, learning and classification. The pattern measurements come from the structural sensors. The objective of the feature extraction is to reduce the number of observation spaces into a manageable size of important feature spaces, so that only the discriminatory information is retained. The feature extraction should optimally retain a minimum number of dimensions while maintaining the maximum probability of correct classification. The features are defined for each application based on physical considerations. The definition of features can take place in either time or frequency domain. Once the dimensions have been reduced, the features are ordered by ranking them. This rank indicates which features are more important for classification purpose. In order to perform the ranking the nearest neighbor rule is suggested. Knowledge of the correct output for several damage scenarios is required for the learning procedure. This information may come from the FEM of the structure. The knowledge acquired in the learning step will be used by the classification procedure. Data that belong to different classes will reside in different regions in the feature

space. Ideally, the classifier will divide the feature space into mutually exclusive regions.

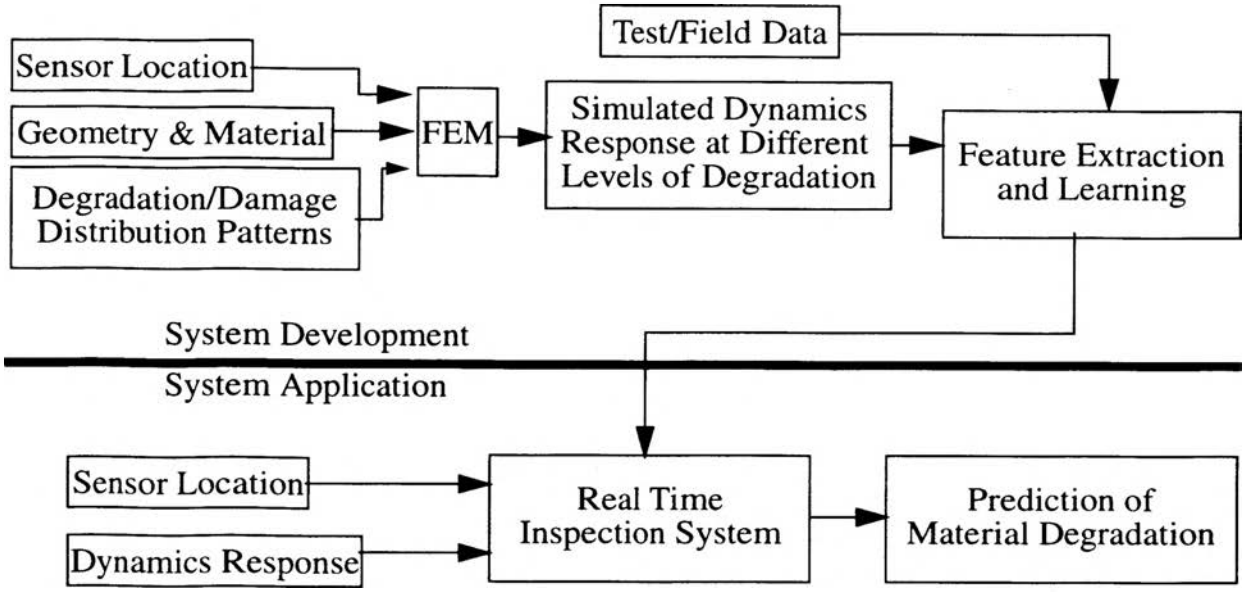

Figure 2. Schematic for damage detection using pattern recognition

In this particular study, three classifiers were considered for the classification of different characteristics; the three classifiers were the Single Gaussian, Fisher Linear Discriminant and the Nearest Neighbor Criteria, and the characteristics that were considered are summarized in Table I, together with the classification options. The feature considered for each characteristic case were different: "Mean Value of the Normalized Enveloped Function" for Damage Status classification; "Mean Value of the Normalized Enveloped Function", "Variance of the Normalized Waveform Amplitude Values" and "Local Fall Variance Between Peak and 25% level" for the classification of Degree of Modulus Degradation; "Difference between 50% level and

25% level (Waveform Cumulative Distribution)" for Damage Zone classification; and "Fraction of total power between lower 50% level and peak", "Local rise variance between 50% level and peak spectrum" and "Globally fall time from peak to 50% level" for the classification of Damage Zone Sizes. In all the cases the Nearest Neighbor Criteria classifier produced the minimum error percentage of classification, but some of these percentages were quite high. The minimum error, 2%, was obtained for the case of damage status and mechanism classification. On the other hand, a higher error was obtained in the classification of the damaged zone sizes into 4 classes, in which a 48% error was experienced.

Table I: Characteristics considered for classification

Characteristic	Classes
Damage Status and Mechanism	2: Undamaged / Modulus Degradation 3: Undamaged / Modulus Degradation/Delamination
Degree of Modulus Degradation	3: Undamaged / <10% degradation / >10% degradation 5: Undamaged / 5% / 10% / 20% / >30%
Damage Zone Location	2: 0" - 3" / 3" - 5"
Damage Zone Size	2: $\leq 2inches$ / $\geq 3inches$ 4: Undamaged / 1"/ 2" / 3" / 4"

Some of the obtained classification errors were relatively high, but this study was performed with a small data base for the learning step. With a more extensive data base, better results will be expected.

D. LOCAL DAMAGE DETECTION USING STRUCTURAL IMPEDANCE

In certain applications it would be beneficial to monitor the integrity of very critical local areas. This should happen in such a way that the monitoring of the local area is not affected by changes in the rest of the structure. This kind of damage detection will be ideal for critical areas such as bolts and junctions.

Chaudhry et al.[12], presents a method to perform local damage detection using piezoelectric (PZT) patches to detect changes in structural impedance at high frequencies. In this study the PZT patches were used as both sensors and actuators. The actuation/sensing capabilities of a PZT patch are limited to a small region close to the patch location, in particular when used at high frequencies. Therefore, the changes in structural impedance that may be detected using a PZT patch at high frequency, corresponds to changes in the local area. At high frequencies, typically greater that 50 KHz, the structural response is dominated by local modes and damages like micro-cracks, loose connections and delamination.

Piezoelectric material exhibits the direct and converse effect. The direct effect is the phenomenon of electric charge generation when the material is subjected to a mechanical stress; and, the converse effect is when a mechanical strain is generated due to an applied electric field. Therefore, PZT patches provide a mean for coupling the electrical and mechanical impedance. The electrical impedance is defined as the ratio of the applied voltage and the resulting current; while the mechanical impedance is the ratio of the applied force and the resulting velocity. The electrical impedance can be measured using an impedance analyzer, which is commercially available. Any change in the local impedance signatures indicates a variation in the

local area structural integrity. This impedance signature idea was applied to detect when a pair of bolts were getting loosen. Considering a 100% damage to be the smallest possible turn on a local area bolt, all local alterations were identified to be greater than 55%. Meanwhile, any change outside the local area resulted in an identified damage of less than 7%.

This kind of approach will allow to detect very small changes, such as micro-cracks and loose bolts. The only problem with the suggested technique is that the electrical properties of the PZT are easily affected by changes in temperature, which may lead to a false diagnosis.

III. MODELING OF BRIDGE-LIKE STRUCTURES

In this section, different methods to obtain a state space model of a bridge-like structure will be discussed. Bridge-like structures are mainly designed and constructed using trusses. The most common method for modeling a structure, including truss structures, is the finite element method. This modeling technique uses the physical parameters of the structural elements as well as the interconnection of the structural elements to determine a mathematical model of the structure. The mass and stiffness matrices of the equation of motion for an n-DOF is obtained from the finite element method. If the structure is lightly damped, the damping may be neglected. For bridge-like structures, in which the damping constitutes a very important factor of the structural response, the damping can be determined from the structural response. Once the equation of motion is known, a state space representation can be determined in which the states represent the displacement and velocity of the structural DOF. This particular state space representation is known as the physical coordinate state space representation. From the state space representation the natural frequencies and mode shapes can be determined. A procedure for determining the natural frequencies and mode shapes will be presented.

In addition to the finite element method, two other methods for obtaining a state space mathematical model of a structure will be reviewed. These two other methods are used to determine a state space representation model of a structure from measured data; in other words, these methods are system identification methods. The first system identification procedure provides for obtaining the state space representation from the swept sine frequency response of the structure. The other

system identification method that will be discussed is the Eigensystem Realization Algorithm (ERA). This system identification method determines a discrete state space representation for the structure from experimental data. In order to estimate a discrete state space representation using the ERA, the Markov parameters (MPs) of the structure should be determined first. A method for determining the MPs of a structure using a feedforward neural network will be reviewed.

Finally, a FEM of a laboratory-scale bridge-like structure will be presented, as well as some of the difficulties encountered with the obtained mathematical model of the structure.

A. FINITE ELELEMENT MODEL OF A TRUSS STRUCTURE

Any structure can be modeled using the finite element method. The mathematical model obtained using the finite element method is known as finite element model (FEM). Most of the bridge-like structures are design and constructed using trusses. Therefore, the procedure for modeling a truss structure using the finite element method will be reviewed[13].

The finite element method is used to model the structural stiffness as well as the structural mass. By doing this, the stiffness matrix and the mass matrix of the equation of motion, Equation (2), are obtained. The structural damping is not modeled by the finite element method. The finite element method divides the structure into a number of structural elements. The way in which these structural elements are interconnected as well as some physical parameters of the structural elements are used to determine the contribution of each structural element to the

global stiffness and mass matrices of the structure. The point where two or more structural elements are joined together is called a node.

For other kind of structures, other than trusses, the FEM can be improved by dividing each structural element into smaller structural elements. This is not the case for truss structures, in which further subdivision of a finite element does not add to the accuracy of the FEM.

The finite element method can be applied to both 2-D (planar) and 3-D structures. In both cases, a global coordinate system is defined in order to determine the mathematical model of the structure; global coordinates are defined for each structural node. The finite element method presented in the following sections considers each structural element behaves as a bar; i.e., the structural element experience longitudinal vibration. The structural elements are assumed to vibrate only along the element axis; while the structure can vibrate in both X and Y directions for a 2-D structure, and in the X, Y and Z directions for a 3-D structure.

1. Finite Element Model of Planar (2-D) Structures The best way to review the finite element method for truss structures is using a simple example. Therefore, consider a three elements planar truss structure with two degrees-of-freedom (DOF) as shown in Figure 3. All the structural elements have cross sectional A and Young's modulus E. The global stiffness and mass matrices are the result of the individual structural elements contribution. Note from Figure 3 that both structural elements and structural nodes have been identified. The degrees of freedom had been identified by dx or dy depending on the direction, and the subscript makes reference to the structural node.

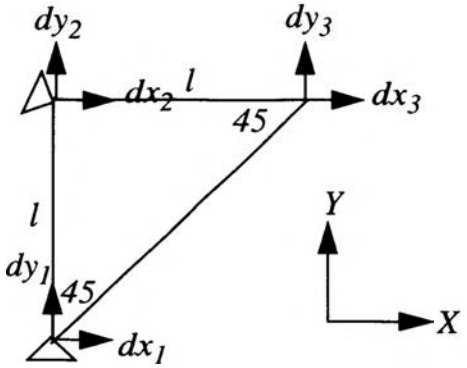

Figure 3. Three elements planar truss structure with 2-DOF

Modeling each structural element as a bar, the contribution of each structural element, K^i, to the global stiffness matrix is determined by the matrix

$$K^i = \frac{A_i E_i}{L_i} \begin{bmatrix} dx_s & dy_s & dx_e & dy_e \\ c^2(\theta_i) & cs(\theta_i) & -c^2(\theta_i) & -cs(\theta_i) \\ cs(\theta_i) & s^2(\theta_i) & -cs(\theta_i) & -s^2(\theta_i) \\ -c^2(\theta_i) & -cs(\theta_i) & c^2(\theta_i) & cs(\theta_i) \\ -cs(\theta_i) & -s^2(\theta_i) & cs(\theta_i) & s^2(\theta_i) \end{bmatrix} \begin{matrix} dx_s \\ dy_s \\ dx_e \\ dy_e \end{matrix} \tag{41}$$

where the subscript i makes reference to the i^{th} structural element, $c(\theta_i)$ and $s(\theta_i)$ respectively represents the cosine and sine of θ_i, θ_i is the angle between the global coordinate X-axis and the axis along the structural element, and the row and column references are dx_s = displacement in the X-direction at the starting structural node, dy_s = displacement in the Y-direction at the starting structural node, dx_e = displacement in the X-direction at the ending structural node and dy_e = displacement in the Y-direction at the ending structural node. Once the matrix K^i has been determined for all the structural elements, the global stiffness matrix can be

assembled. All the matrices elements with the same column and row references are added together and placed in the respective location at the global matrices; so that, the stiffness matrix for the structure shown in Figure 3 is

$$K = \begin{array}{c} \begin{matrix} dx_1 & dy_1 & dx_2 & dy_2 & dx_3 & dy_3 \end{matrix} \\ \begin{bmatrix} K^2_{11}+K^3_{11} & K^2_{12}+K^3_{12} & K^3_{13} & K^3_{14} & K^2_{13} & K^2_{14} \\ K^2_{12}+K^3_{12} & K^2_{22}+K^3_{22} & K^3_{23} & K^3_{24} & K^2_{23} & K^2_{24} \\ K^3_{13} & K^3_{23} & K^1_{11}+K^3_{33} & K^1_{12}+K^3_{34} & K^1_{13} & K^1_{14} \\ K^3_{14} & K^3_{24} & K^1_{12}+K^3_{34} & K^1_{22}+K^3_{44} & K^1_{23} & K^1_{24} \\ K^2_{13} & K^2_{23} & K^1_{13} & K^1_{23} & K^1_{33}+K^2_{33} & K^1_{34}+K^2_{34} \\ K^2_{14} & K^2_{24} & K^1_{14} & K^1_{24} & K^1_{34}+K^2_{34} & K^1_{44}+K^2_{44} \end{bmatrix} \end{array} \begin{matrix} dx_1 \\ dy_1 \\ dx_2 \\ dy_2 \\ dx_3 \\ dy_3 \end{matrix} . \quad (42)$$

From Figure 3 it can be observed that the displacements dx_1, dy_1, dx_2 and dy_2 are equal to zero. Therefore, their corresponding columns and rows are to be deleted; so that, the global stiffness matrix is

$$K = \begin{array}{c} \begin{matrix} dx_3 & dy_3 \end{matrix} \\ \begin{bmatrix} K^1_{33}+K^2_{33} & K^1_{34}+K^2_{34} \\ K^1_{34}+K^2_{34} & K^1_{44}+K^2_{44} \end{bmatrix} \end{array} \begin{matrix} dx_3 \\ dy_3 \end{matrix} . \quad (43)$$

The global mass matrix can be determined using the so called consistent mass method or the lumped mass method. The consistent mass method follows a similar procedure to the reviewed procedure for the stiffness; with the difference that each structural element contribution, M^i, is determined from

$$M^i = \frac{\rho_i A_i L_i}{6} \begin{bmatrix} dx_s & dy_s & dx_e & dx_e \\ 2c^2 & 2cs & c^2 & cs \\ 2cs & 2s^2 & cs & s^2 \\ c^2 & cs & 2c^2 & 2cs \\ cs & s^2 & 2cs & 2s^2 \end{bmatrix} \begin{matrix} dx_s \\ dy_s \\ dx_e \\ dx_e \end{matrix} . \tag{44}$$

Using the lumped mass matrix procedure, each structural element contribution, M^i, is determined from

$$M^i = \frac{\rho_i A_i L_i}{2} \begin{bmatrix} dx_s & dx_e \\ dy_s & dy_e \\ 1\ 0 & 0\ 0 \\ 0\ 1 & 0\ 0 \\ 0\ 0 & 1\ 0 \\ 0\ 0 & 0\ 1 \end{bmatrix} \begin{matrix} dx_s \\ dy_s \\ dx_e \\ dy_e \end{matrix} . \tag{45}$$

Once the individual structural elements contribution are determined, either by using the consistent or lumped mass method, the global mass matrix is assembled adding all the matrices elements with the same columns and rows references. Doing this, the global mass matrix for the structure shown in Figure 3 is

$$M = \begin{matrix} \\ dx_1 \\ dy_1 \\ dx_2 \\ dy_2 \\ dx_3 \\ dy_3 \end{matrix} \begin{bmatrix} dx_1 & dy_1 & dx_2 & dy_2 & dx_3 & dy_3 \\ M_{11}^2 + M_{11}^3 & M_{12}^2 + M_{12}^3 & M_{13}^3 & M_{14}^3 & M_{13}^2 & M_{14}^2 \\ M_{12}^2 + M_{12}^3 & M_{22}^2 + M_{22}^3 & M_{23}^3 & M_{24}^3 & M_{23}^2 & M_{24}^2 \\ M_{13}^3 & M_{23}^3 & M_{11}^1 + M_{33}^3 & M_{12}^1 + M_{34}^3 & M_{13}^1 & M_{14}^1 \\ M_{14}^3 & M_{24}^3 & M_{12}^1 + M_{34}^3 & M_{22}^1 + M_{44}^3 & M_{23}^1 & K_{24}^1 \\ M_{13}^2 & M_{23}^2 & M_{13}^1 & M_{23}^1 & M_{33}^1 + M_{33}^2 & M_{34}^1 + M_{34}^2 \\ M_{14}^2 & M_{24}^2 & M_{14}^1 & M_{24}^1 & M_{34}^1 + M_{34}^2 & M_{44}^1 + M_{44}^2 \end{bmatrix} . \tag{46}$$

Applying the boundary conditions, the global mass matrix is

$$M = \begin{bmatrix} dx_3 & dy_3 \\ M_{33}^1 + M_{33}^2 & M_{34}^1 + M_{34}^2 \\ M_{34}^1 + M_{34}^2 & M_{44}^1 + M_{44}^2 \end{bmatrix} \begin{matrix} dx_3 \\ dy_3 \end{matrix}. \tag{47}$$

Using the lumped mass matrix method provides less accurate result than using the consistent mass method, but it provides a simple way to add extra masses attached to the structure, such as actuators. This flexibility, is due to the fact that the lumped mass method assign to each structural node half of the mass of each structural element connected to it. So that, if an extra mass is present in the structure, its mass will be assigned to the closest structural node.

2. Finite Element Model of 3-D Structures The discussed procedure for a planar structure can be extended for a 3-D structure. On a 3-D structure, there are up-to 3 possible DOF at each structural node; a 3-D global coordinate is defined at each structural element. The contribution of each structural element, K^i, to the global stiffness matrix is determined using the matrix

$$K^i = \frac{A_i E_i}{L_i} \begin{bmatrix} dx_s & dy_s & dz_s & dx_e & dy_e & dz_e \\ c_{x_i}^2 & c_{x_i}c_{y_i} & c_{x_i}c_{z_i} & -c^2{}_{x_i} & -c_{x_i}c_{y_i} & -c_{x_i}c_{z_i} \\ c_{x_i}c_{y_i} & c^2{}_{y_i} & c_{y_i}c_{z_i} & -c_{x_i}c_{y_i} & -c^2{}_{y_i} & -c_{y_i}c_{z_i} \\ c_{x_i}c_{z_i} & c_{y_i}c_{z_i} & c^2{}_{z_i} & -c_{x_i}c_{z_i} & -c_{y_i}c_{z_i} & -c^2{}_{z_i} \\ -c^2{}_{x_i} & -c_{x_i}c_{y_i} & -c_{x_i}c_{z_i} & c^2{}_{x_i} & c_{x_i}c_{y_i} & c_{x_i}c_{z_i} \\ -c_{x_i}c_{z_i} & -c^2{}_{y_i} & -c_{y_i}c_{z_i} & c_{x_i}c_{y_i} & c^2{}_{y_i} & c_{y_i}c_{z_i} \\ -c_{x_i}c_{z_i} & -c_{y_i}c_{z_i}' & -c^2{}_{z_i} & c_{x_i}c_{z_i} & c_{y_i}c_{z_i} & c^2{}_{z_i} \end{bmatrix} \begin{matrix} dx_s \\ dy_s \\ dz_s \\ dx_e \\ dy_e \\ dz_e \end{matrix}, \tag{48}$$

where θ_{x_i}, θ_{y_i} and θ_{z_i} are the respective angles between the i^{th} structural element and the global coordinate *X*-, *Y*- and *Z*-axis. Once the individual contribution matrix, K^i, has been determined for all the structural elements, the global stiffness matrix may be assembled using the same procedure used for the 2-D structure; in which, all the matrices elements with the same row and column references are added together and placed in their respective matrix location. After assembling the global stiffness matrix, the boundary conditions are considered to reduce the order of the global stiffness matrix eliminating the row and column corresponding to the fixed DOF.

For a 3-D structure, there is also the option of using the consistent mass method or the lumped mass method. In order to determine the contribution of each structural element to the global mass matrix using the consistent matrix method, the following matrix is considered

$$M^i = \frac{\rho_i A_i L_i}{2} \begin{array}{c} \begin{matrix} dx_s & dy_s & dz_s & dx_e & dy_e & dz_e \end{matrix} \\ \begin{bmatrix} 2c^2_{x_i} & 2c_{x_i}c_{y_i} & 2c_{x_i}c_{z_i} & c^2_{x_i} & c_{x_i}c_{y_i} & c_{x_i}c_{z_i} \\ 2c_{x_i}c_{y_i} & 2c^2_{y_i} & 2c_{y_i}c_{z_i} & c_{x_i}c_{y_i} & c^2_{y_i} & c_{y_i}c_{z_i} \\ 2c_{x_i}c_{z_i} & 2c_{y_i}c_{z_i} & 2c^2_{z_i} & c_{x_i}c_{z_i} & c_{y_i}c_{z_i} & c^2_{z_i} \\ c^2_{x_i} & c_{x_i}c_{y_i} & c_{x_i}c_{z_i} & 2c^2_{x_i} & 2c_{x_i}c_{y_i} & 2c_{x_i}c_{z_i} \\ c_{x_i}c_{y_i} & c^2_{y_i} & c_{y_i}c_{z_i} & 2c_{x_i}c_{y_i} & 2c^2_{y_i} & 2c_{y_i}c_{z_i} \\ c_{x_i}c_{z_i} & c_{y_i}c_{z_i} & c^2_{z_i} & 2c_{x_i}c_{z_i} & 2c_{y_i}c_{z_i} & 2c^2_{z_i} \end{bmatrix} \begin{matrix} dx_s \\ dy_s \\ dz_s \\ dx_e \\ dy_e \\ dz_e \end{matrix} \end{array} . \tag{49}$$

Using the lumped mass method the individual contribution to the global mass matrix is determined by the matrix

$$M^i = \frac{\rho_i A_i L_i}{2} \begin{array}{c} \begin{matrix} dx_s & dz_s & dy_e \\ dy_s & dx_e & dz_e \end{matrix} \\ \begin{bmatrix} 1 & 0 & 0 & 0 & 0 & 0 \\ 0 & 1 & 0 & 0 & 0 & 0 \\ 0 & 0 & 1 & 0 & 0 & 0 \\ 0 & 0 & 0 & 1 & 0 & 0 \\ 0 & 0 & 0 & 0 & 1 & 0 \\ 0 & 0 & 0 & 0 & 0 & 1 \end{bmatrix} \end{array} \begin{matrix} dx_s \\ dy_s \\ dz_s \\ dx_e \\ dy_e \\ dz_e \end{matrix} . \tag{50}$$

Using the matrices M^i for all the structural elements, the global mass matrix is assembled using the same procedure used for the stiffness matrix.

The individual contribution matrices, K^i and M^i, are determined using some physical properties of each structural element as well as the location of the nodes to which each structural element is attached. Modeling each structural element as bar, the required physical properties for modeling a structure using the finite element method are the elements cross sectional area, Young's modulus and density. Considering a structural element to be attached to the structural nodes a and b; note that, the same global mass and stiffness matrices will be obtained if the structural element is consider to go either from a to b, or from b to a.

3. Computation of Natural Frequencies and Mode Shapes Having modeled the mass and stiffness of a lightly damped structure, the structural response to external forces can be determined using the equation of motion for an n-DOF structure

$$M\ddot{x} + Kx = f. \tag{51}$$

where x is the vector of the DOF displacement, $\ddot{x}$ is the vector of the DOF acceleration and f is the vector of external forces. From Equation (51), the physical coordinate state space representation is found to be

$$\begin{bmatrix} \dot{x}_1 \\ \dot{x}_2 \end{bmatrix} = \begin{bmatrix} 0 & I \\ -M^{-1}K & 0 \end{bmatrix} \begin{bmatrix} x_1 \\ x_2 \end{bmatrix} + \begin{bmatrix} 0 \\ M^{-1} \end{bmatrix} f \Leftrightarrow \dot{x} = Ax + Bf . \tag{52}$$

The structural natural frequencies and mode shapes can be obtained by solving the algebraic eigenvalue problem[13]

$$Az = \lambda z, \; z \neq 0 . \tag{53}$$

The obtained $2n$ eigenvalues, λ_g, of the matrix A are related to the structural natural frequencies by the equation

$$\lambda_g = \pm j\omega_i , \tag{54}$$

where $g = 1, 2, \ldots, 2n$, $i = 1, 2, \ldots, n$, $j = \sqrt{-1}$ and ω_i is the natural frequency for the i^{th} mode. And the obtained $2n$ eigenvectors, z_g, of the matrix A are related to the structural mode shapes by

$$z_g = \begin{bmatrix} u_i \\ \lambda u_i \end{bmatrix} , \tag{55}$$

where u_i are the structural mode shapes.

For the case of an n-DOF damped structure, the equation of motion is given by

$$M\ddot{q} + D\dot{q} + Kq = f(t) . \tag{56}$$

Expressing Equation (56) in the physical coordinate state space representation,

$$\begin{bmatrix} \dot{x}_1 \\ \dot{x}_2 \end{bmatrix} = \begin{bmatrix} 0 & I \\ -M^{-1}K & -M^{-1}D \end{bmatrix} \begin{bmatrix} x_1 \\ x_2 \end{bmatrix} + \begin{bmatrix} 0 \\ M^{-1} \end{bmatrix} f \Leftrightarrow \dot{x} = Ax + Bf . \tag{57}$$

Due to the damping, the eigenvalues and eigenvectors of the matrix A, λ_g and z_g respectively, may be complex; causing the mode shapes, u_i, to be complex. The

physical interpretation of the complex eigenvalues λ_g is the same as the interpretation for an underdamped single DOF, so that

$$\lambda_g = -\zeta_i\omega_i \pm j\omega_i\sqrt{1-\zeta^2}, \tag{58}$$

where ω_i is the underdamped natural frequency for the i^{th} mode, and ζ_i is the modal damping ratio of the i^{th} mode. Considering $\lambda_g = \alpha_g + j\beta_g$, the underdamped natural frequencies and modal damping ratios are determined to be

$$\omega_i = \sqrt{\alpha_g^2 + \beta_g^2} \tag{59}$$

and

$$\zeta_i = -\frac{\alpha_g}{\sqrt{\alpha_g^2 + \beta_g^2}}. \tag{60}$$

In terms of complex mode shapes, each element describes the relative motion magnitude and phase of the DOF associated with that element when the structure is excited at the corresponding natural frequency.

B. DERIVATION OF STATE SPACE MODELS FROM EXPERIMENTAL DATA

A state space representation of a structure can be obtained using the swept sine frequency response of the structure, or by using the Eigensystem Realization Algorithm (ERA)[14]. These two methods of system identification will be reviewed in the following sections.

1. State Space Representation From Frequency Response The frequency response of a structure can be determined using the so called swept sine method. From this test a magnitude and a phase plot are obtained, which represent the structural

frequency response. These plots can be curve fitted by placing poles and zeros, in such a way that the frequency response of the generated transfer function is as close as possible to the obtained from the swept sine test. One transfer function needs to be determined for each input-output relationship. Once this has been achieved, the generated transfer function can be used to generate a state space representation of the structure by using any of the standard procedures for canonical state space representation from transfer function, such as the controller canonical form. Consider the generated transfer function $G(s)$ to be

$$G(s) = \frac{b_1 s^{n-1} + b_2 s^{n-2} + \ldots + b^n}{s^n + a_1 s^{n-1} + \ldots + a_n}. \tag{61}$$

Then the state space controller canonical form representation is

$$\dot{x} = \begin{bmatrix} -a_1 & -a_2 & \ldots & -a_n \\ 1 & 0 & \ldots & 0 \\ 0 & 1 & 0 & \ldots \\ \ldots & 0 & \ldots & 0 \\ 0 & \ldots & 0 & 1 \end{bmatrix} x + \begin{bmatrix} 1 \\ 0 \\ \ldots \\ 0 \end{bmatrix} f \tag{62}$$

$$y = \begin{bmatrix} b_1 & b_2 & \ldots & b_n \end{bmatrix} x, \tag{63}$$

where x is the state vector, f is the input vector, and y is the measurement of the states.

If the state space representation is to be used in damage detection, it should correspond to the physical coordinate representation. The controller canonical form does not satisfy this condition. Therefore, a linear transformation needs to be found which transforms the controller canonical form into the physical coordinate

representation. A procedure to transform any arbitrary state space representation into the physical coordinate will be proposed in Section IV.B.

2. State Space Representation Using The Eigensystem Realization Algorithm The ERA method has been successfully applied in the modeling of smart structures[15,16]. This method determines a minimal order discrete-time state space representation of a system from its Markov parameters (MPs).

Knowing the structural response to a uniformly distributed random input, the MPs of the structure can be determined by using an observer formulation[17] and/or by using a feedforward neural network[18]. The feedforward neural network method is preferred[15] over the observer formulation because training a feedforward neural network is less computationally intensive than the computations required for the observer formulation; and, more accurate estimation of the MPs is achieved when dealing with noisy experimental data (due to the noise rejection properties of neural networks).

a. Markov parameters calculation using neural networks An N^{th} order linear discrete-time system described by the state space representation

$$x(k+1) = Ax(k) + Bu(k) \tag{64}$$

$$y(k) = Cx(k) \tag{65}$$

can also be described in terms of its MPs,

$$y(k) = \left[CA^0B \;\; CA^1B \;\ldots\; CA^{N-1}B\right] \times [Z^{-1}[u(k)]], \tag{66}$$

where $CA^{n-1}B$ for $n = 1, 2, \ldots, N$ are the system MPs; and $Z^{-1}[u(k)]$ represents past inputs to the system

$$Z^{-1}[u(k)] = \begin{bmatrix} u(k) \\ u(k-1) \\ \cdots \\ u(k-N+1) \end{bmatrix}_{N \times 1} . \tag{67}$$

A mapping of the structural-input to the structural-output (response) can be obtained using a multilayered feedforward neural network, as shown in Figure 4.

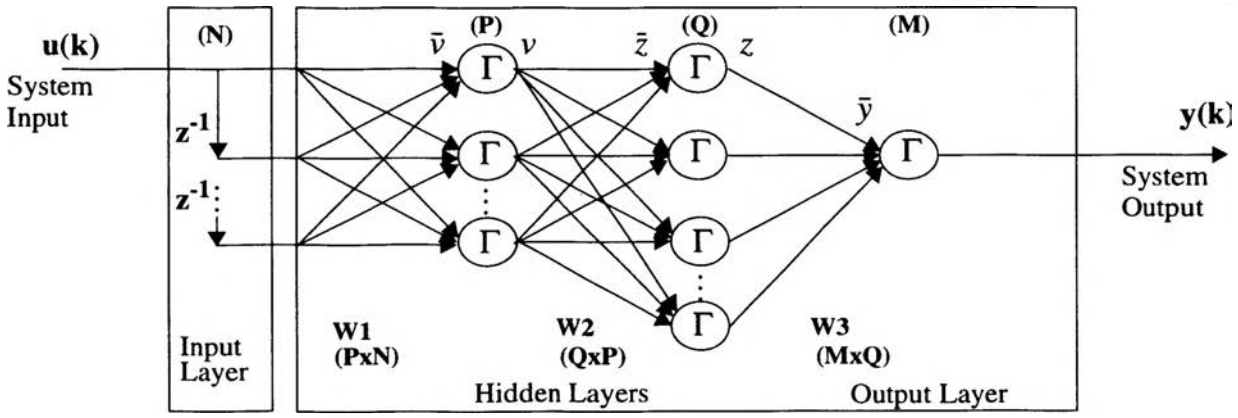

Figure 4. Neural network architecture for Markov parameter calculation

Once the network has been trained, it will map the input $Z^{-1}[u(k)]$ into the output

$$y(k) = \xi \times W_3 \times \Gamma(W_2 \times \Gamma(W_1 \times Z^{-1}[u(k)])) \tag{68}$$

where W_1, W_2 and W_3 are the weighting matrices of the network, and ξ is a constant. Considering that post-training the neurons can be assumed to operate in the linear range of the nonlinear activation function, $y(k)$ can be expressed as

$$y(k) = \xi \times W_3 \times W_2 \times W_1 . \tag{69}$$

Comparing equations (3) and (6), it can be observed that for a proper choice of N (number of past inputs of the system, the MPs are proportional to the product of the network weighting matrices. This can be expressed as

$$\xi \times W_3 \times W_2 \times W_1 = \left[CA^0B \quad CA^1B \quad \ldots \quad CA^{N-1}B \right]. \tag{70}$$

Therefore, a multilayered feedforward neural network can be used to determine the MPs of a structure.

b. Eigensystem Realization Algorithm The Hankel matrix, $H_{rs}(\tau-1) \in \Re^{r \times s}$, is formed using the MPs $Y(\tau)$ of a physical structure

$$H_{rs}(\tau-1) = \begin{bmatrix} Y(\tau) & Y(\tau+1) & \ldots & Y(\tau+s-1) \\ Y(\tau+1) & Y(\tau+2) & \ldots & \ldots \\ \ldots & \ldots & \ldots & \ldots \\ Y(\tau+r-1) & \ldots & \ldots & Y(\tau+r+s-1) \end{bmatrix} \tag{71}$$

Nonsingular matrices U and V, and diagonal matrix S can be obtained by performing the singular value decomposition to $H_{rs}(0)$,

$$H_{rs}(0) = U \times S \times V^T \tag{72}$$

If S contains n nonzero singular values, and the structure has m inputs and q outputs, then the matrices U, S and V can be truncated to $U_1 \in \Re^{rq \times n}$, $S_1 \in \Re^{n \times n}$ and $V_1 \in \Re^{m \times s}$, so that

$$H_{rs}(0) = U_1 \times S_1 \times V_1^T . \tag{73}$$

Defining E_q and E_m to be

$$E_q = \left[I_q \; 0_q \; \ldots \; 0_q \right] \tag{74}$$

$$E_m = \left[I_m \; 0_m \; \ldots \; 0_m \right] \tag{75}$$

where $0_q = 0 \in \Re^{x \times q}$ and $0_m = 0 \in \Re^{x \times m}$, the n^{th} order identified system has the following discrete state space matrices

$$A_{id} = S_1^{-1/2} U_1^T H_{rs}(1) V_1 S_1^{-1/2} \tag{76}$$

$$B_{id} = S_1^{1/2} V_1^T E_m \tag{77}$$

$$C_{id} = E_q^T U_1 S_1^{1/2} \tag{78}$$

Thus, the identified structure can be described by the discrete equations

$$x(k+1) = Ax(k) + Bu(k) \tag{79}$$

$$y(k) = Cx(k). \tag{80}$$

Note that the proposed global damage detection method has been developed using the continuous state space representation of the structure. Additionally, it should be recalled that the state space representation of any system is not unique. Therefore, it is required to transform the identified state space representation into the physical coordinates of the structure. A method to achieve this linear transformation will be proposed.

C. FEM OF A LABORATORY BRIDGE-LIKE STRUCTURE

A truss structure with 18-DOF was setup at the University of Missouri-Rolla Intelligent System Center Health Monitoring Laboratory for damage detection experimentation. A diagram of the structural system is shown in Figure 5. Structural

elements 1 thru 14 are aluminum rods, while the structural elements 15 thru 17 consist of a stainless steel bolt (radius = 0.125 *in*), surrounded by an aluminum cylinder (radius = 0.125 *in*). For modeling the structural stiffness, these structural elements are considered to be stainless steel rods, with radius = 0.25 *in*. Some physical properties of the structural elements are summarized in Table II.

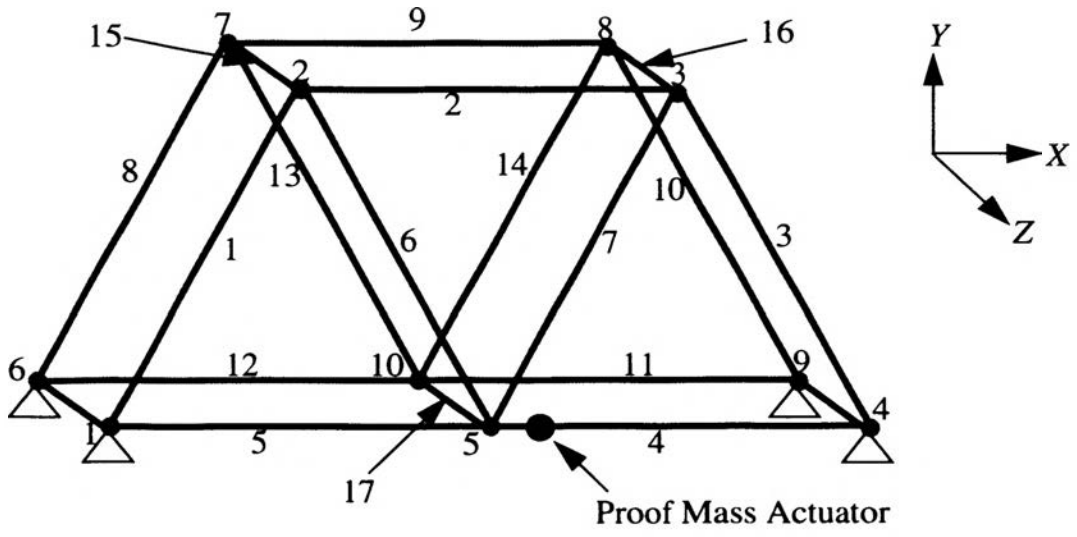

Figure 5. Truss structure used for damage detection experimentation

Table II: Physical properties of the structural elements

Physical Property	Aluminum Element	Stainless Steel Element
Cross Sectional Area (in^2)	196.4×10^{-3}	196.4×10^{-3}
Young's Modulus (*psi*)	10.2×10^{6}	30×10^{6}
Length (*in*)	14	4.5
Density(# sec^2/in^4)	245.9×10^{-6}	

The mass of the bolts, aluminum cylinders and actuator were determined using a mass scale, while the mass of the aluminum rods were determined using the relationship $M = \rho AL$. The mass information is summarized in Table III. The stiffness and mass constants, $k^i = \frac{A_i E_i}{L_i}$ and $m^i = \frac{\rho_i A_i L_i}{2}$, for all the structural elements are provided in Table IV.

Table III: Mass of the structural components

Structural Component	mass (# sec^2/in)
Aluminum Cylinder	299.7×10^{-6}
Stainless Steel Bolts	225.9×10^{-6}
Proof Mass Actuator	1147.6×10^{-6}
Aluminum Rods	676.6×10^{-6}

Table IV: Stiffness and mass constants of the structural elements

Structural Element	$k^i = \frac{A_i E_i}{L_i}$ (#/in)	$m^i = \frac{\rho_i A_i L_i}{2}$ (# sec^2/in)
1-14	143.1×10^{3}	338.3×10^{-6}
15-17	1.31×10^{6}	262.8×10^{-6}

The proof mass actuator consists of a mass attached to a base which contains piezoelectric material. So, the applied force can be controlled by the applied voltage

to the actuators terminals. In order to measure the response of the structure, 6 accelerometers were placed at different DOF: dx_2, dy_2, dy_3, dy_5, dy_7 and dx_8, where x and y represent the axis in which direction the sensor has been placed, and the number in the subscript represents the structural node at which the sensor has been placed. Note that the mass of the actuator is very significant when compared to the mass of the structural elements; in fact, it adds more mass to the structure than any structural element. Therefore, the mass of the actuator must be considered in the FEM; this can be accomplish by modeling the structural mass using the lumped mass method. The nodes to which the structural elements are connected, as well as the angles between the structural elements and the global coordinate axis are provided in Table V.

Table V: Structural elements connections and angles with axis

Structural Element	Connected to Nodes	θ_{x_i}	θ_{y_i}	θ_{z_i}
1	1,2	60	30	90
2	2,3	0	90	90
3	3,4	120	-30	90
4	4,5	0	90	90
5	1,5	0	90	90
6	2,6	120	-30	90
7	3,5	60	30	90
8	6,7	60	30	90
9	7,8	0	90	90
10	8,9	120	-30	90

Table V: Structural elements connections and angles with axis

Structural Element	Connected to Nodes	θ_{x_i}	θ_{y_i}	θ_{z_i}
11	9,10	0	90	90
12	6,10	0	90	90
13	7,10	120	-30	90
14	8,10	60	30	90
15	2,7	90	90	180
16	3,8	90	90	180
17	5,10	90	90	180

Using Equation (48), the contribution of the structural elements to the global stiffness matrix are

$$K^{1,7,8,14} = k^i \begin{bmatrix} 0.25 & 0.433 & 0 & -0.25 & -0.433 & 0 \\ 0.433 & 0.75 & 0 & -0.433 & -0.75 & 0 \\ 0 & 0 & 0 & 0 & 0 & 0 \\ -0.25 & -0.433 & 0 & 0.25 & 0.433 & 0 \\ -0.433 & -0.75 & 0 & 0.433 & 0.75 & 0 \\ 0 & 0 & 0 & 0 & 0 & 0 \end{bmatrix}, \tag{81}$$

$$K^{2,4,5,9,11,12} = k^i \begin{bmatrix} 1 & 0 & 0 & -1 & 0 & 0 \\ 0 & 0 & 0 & 0 & 0 & 0 \\ 0 & 0 & 0 & 0 & 0 & 0 \\ -1 & 0 & 0 & 1 & 0 & 0 \\ 0 & 0 & 0 & 0 & 0 & 0 \\ 0 & 0 & 0 & 0 & 0 & 0 \end{bmatrix}, \tag{82}$$

$$K^{3,\,6,\,10,\,13} = k^{i}\begin{bmatrix} 0.25 & -0.433 & 0 & -0.25 & 0.433 & 0 \\ -0.433 & 0.75 & 0 & 0.433 & -0.75 & 0 \\ 0 & 0 & 0 & 0 & 0 & 0 \\ -0.25 & 0.433 & 0 & 0.25 & -0.433 & 0 \\ 0.433 & -0.75 & 0 & -0.433 & 0.75 & 0 \\ 0 & 0 & 0 & 0 & 0 & 0 \end{bmatrix} \tag{83}$$

and

$$K^{15,\,16,\,17} = k^{i}\begin{bmatrix} 0 & 0 & 0 & 0 & 0 & 0 \\ 0 & 0 & 0 & 0 & 0 & 0 \\ 0 & 0 & 1 & 0 & 0 & -1 \\ 0 & 0 & 0 & 0 & 0 & 0 \\ 0 & 0 & 0 & 0 & 0 & 0 \\ 0 & 0 & -1 & 0 & 0 & 1 \end{bmatrix}. \tag{84}$$

Note that there are several elements with the same stiffness contribution matrix, but the difference lie on the row and column references. These references are determine using Equation (48), together with angles provided in Table IV. The stiffness contributions had been determined. Combining the contribution of the individual structural elements by adding the elements which have the same references, and eliminating the rows and columns corresponding to the restricted DOF, the global stiffness matrix is found to be

$$K = \begin{bmatrix} K_{11} & K_{12} \\ K_{21} & K_{22} \end{bmatrix}, \tag{85}$$

where

$$K_{11} = 10^3 \begin{bmatrix} 214.6 & 0 & 0 & -143.1 & 0 & 0 & -35.8 & 61.9 & 0 \\ 0 & 214.6 & 0 & 0 & 0 & 0 & 61.9 & -107.3 & 0 \\ 0 & 0 & 1309.0 & 0 & 0 & 0 & 0 & 0 & 0 \\ -143.1 & 0 & 0 & 214.6 & 0 & 0 & -35.8 & -61.9 & 0 \\ 0 & 0 & 0 & 0 & 214.6 & 0 & -61.9 & -107.3 & 0 \\ 0 & 0 & 0 & 0 & 0 & 1309.0 & 0 & 0 & 0 \\ -35.8 & 61.9 & 0 & -35.8 & -61.9 & 0 & 357.6 & 0 & 0 \\ 61.9 & -107.3 & 0 & -61.9 & -107.3 & 0 & 0 & 214.6 & 0 \\ 0 & 0 & 0 & 0 & 0 & 0 & 0 & 0 & 1309.0 \end{bmatrix}, \quad (86)$$

$$K_{12} = 10^6 \begin{bmatrix} 0 & 0 & 0 & 0 & 0 & 0 & 0 & 0 & 0 \\ 0 & 0 & 0 & 0 & 0 & 0 & 0 & 0 & 0 \\ 0 & 0 & -1.31 & 0 & 0 & 0 & 0 & 0 & 0 \\ 0 & 0 & 0 & 0 & 0 & 0 & 0 & 0 & 0 \\ 0 & 0 & 0 & 0 & 0 & 0 & 0 & 0 & 0 \\ 0 & 0 & 0 & 0 & 0 & -1.31 & 0 & 0 & 0 \\ 0 & 0 & 0 & 0 & 0 & 0 & 0 & 0 & 0 \\ 0 & 0 & 0 & 0 & 0 & 0 & 0 & 0 & 0 \\ 0 & 0 & 0 & 0 & 0 & 0 & 0 & 0 & -1.31 \end{bmatrix}, \quad (87)$$

$$K_{21} = K_{12} \quad (88)$$

and

$$K_{22} = K_{11}. \quad (89)$$

The order of the DOF in the stiffness matrix is: [dx_2, dy_2, dz_2, dx_3, dy_3, dz_3. dx_5, dy_5, dz_5, dx_7, dy_7, dz_7, dx_8, dy_8, dz_8, dx_{10}, dy_{10}, dz_{10}].

In order to model the structural mass, the lumped mass method was used because its flexibility for considering the effect of the proof mass actuator. The expression for the global mass matrix can be obtained observing Figure 5. The mass at the nodes 2,3,7 and 8 are the same: 3/2 the mass of an aluminum rod plus 1/2 the mass of the stainless steel bolt plus 1/2 the mass of the aluminum cylinder. This

mass will be used for the three DOF at each node; i.e., dx_i, dy_i, dz_i. The mass at node 10 is two times the mass of an aluminum rod plus 1/2 the mass of the stainless steel bolt plus 1/2 the mass of the aluminum cylinder. Finally, the mass at node 5 is equal to the mass at node plus the mass of the actuator. Therefore, the diagonal of the global lumped mass matrix is

$$diag(M) = 10^{-6}\begin{bmatrix} (1277.7 \otimes \begin{bmatrix} 1 & 1 & 1 & 1 & 1 & 1 \end{bmatrix})^T \\ (2763.6 \otimes \begin{bmatrix} 1 & 1 & 1 \end{bmatrix})^T \\ (1277.7 \otimes \begin{bmatrix} 1 & 1 & 1 & 1 & 1 & 1 \end{bmatrix})^T \\ (1616.0 \otimes \begin{bmatrix} 1 & 1 & 1 \end{bmatrix})^T \end{bmatrix}, \tag{90}$$

where the operator $m \otimes n$ represents m Kronecker product with n[1].

Note that both global stiffness and mass matrices have been determined. Therefore, the natural frequencies of the structure can be determined using the reviewed procedure in Section III. Using the eigenvalues of the matrix

$$A = \begin{bmatrix} 0_{18\times 18} & I_{18} \\ -M^{-1}K & 0_{18\times 18} \end{bmatrix} \tag{91}$$

for determining the structural natural frequencies, it was obtained that the natural frequencies are: 0, 0, 0, 778.21, 931.88, 1069.33, 1095.38, 1650.78, 1833.05, 2255.70, 2298.51, 2422.57, 2593.86, 2726.37, 2825.49, 5704.50, 7207.39, 7207.39 *Hz*. Note that, when the eigenvalues are determined using the relationship in Equation (54), the units are *rad/s*; in order to get the natural frequencies in *Hz*, the

1. Consider the following example: $a_{1\times 1} \otimes \begin{bmatrix} 1 & 1 & \cdots & 1 \end{bmatrix}_{1\times q} = \begin{bmatrix} a & a & \cdots & a \end{bmatrix}_{1\times q}$.

natural frequencies in *rad/s* are divided by 2π. A swept sine test was performed on the structure to verify the obtained natural frequencies. The obtained frequency response is presented in APPENDIX B, where the frequency response captured by the six accelerometers are presented. As it can be seen from these plots, there are certain peaks in the magnitude which certainly represent natural frequencies. The two peaks which better indicate the presence of natural frequencies are better observed in the frequency response captured by the sensors at the DOF *2-X and 7-Y.* These two natural frequencies correspond to 176.7 and 237.3 *Hz*. The swept sine test indicates the presence of at least two modes in the range of 170 and 245 *Hz*, while the obtained model predicted the first none-zero frequency to occur at 778.21 *Hz*. The three zero natural frequencies are related to a rigid body behavior.

From the obtained results, a significant discrepancy is found between the natural frequencies predicted by the FEM and the experimental natural frequencies. Using the lumped mass method to model the global structural mass introduces a certain level of inaccuracy. The lumped mass method was used to include the effect of the proof mass actuator. The need to include the actuator may be avoided if a shaker is used to excite the structure, and the shaker is attached to the structure through a stinger. The stinger will isolate the shaker from the structure, minimizing the extra load added to the structure. Another possible factor to such a large discrepancy may have been that the actual structural element differs from the bar model used by the applied finite element method; probably, in the actual system the structural elements allow some kind of bending, resulting in unmodeled dynamics.

The bar model used by the finite element method only expands and contract along its axis.

Due to the large discrepancy between the obtained model and the experimental results, this model could not be used for damage detection purpose. Considering the swept sine frequency response, as shown in APPENDIX B, for determining a state space representation is almost impossible, due to the fact that many peaks are present which can not be classified as natural frequencies or not. Given these difficulties with the structure at the laboratory, the damage detection method proposed in this thesis was applied to a simulated structure.

IV. DAMAGE DETECTION USING STATE SPACE MODELS

The damping plays an important role in bridge-like structures. Therefore, a global damage detection and classification method for these kind of structures should address the possible reduction of the structural element damping factors. A global damage detection method in the state space domain is introduced, it addresses both the reduction in damping factor as well as the reduction in stiffness of the structural elements. The proposed algorithm assumes the mass of the structural elements do not change due to the damage. Note this is a feasible assumption for the bridge-like structures, whose structural elements are big and heavy. The proposed global damage detection algorithm (GDDA) is based on the physical coordinate state space representation of the structure. In this particular state space representation, the state variables represent the displacement and the velocity of the structural degrees-of-freedom (DOF).

The proposed damage detection method requires the structural models in the physical coordinate state space representation, hence a transformation matrix is developed for converting any arbitrary state space representation into the physical coordinate system. The proposed linear transformation method is demonstrated for two and three-DOF structures. From these results, the procedure for a general n-DOF structure is also developed. In order to derive mathematical models of the structures from experimental data, the Eigensystem Realization Algorithm (ERA) has been utilized. This algorithm requires the Markov parameters of the structural response; these may be determined using a feedforward neural network architecture. This identified discrete time model has to be converted into the continuous time

domain before it can be converted to the physical coordinate system and used for damage detection purposes.

A. DAMAGE DETECTION USING STATE VARIABLE MODELS

The structural dynamics for an n degrees-of-freedom (DOF) system can be represented by the ordinary differential equation of motion

$$M\ddot{q} + D\dot{q} + Kq = f(t) \tag{92}$$

where M = mass matrix, $M \in \Re^{n \times n}$; D = damping matrix, $D \in \Re^{n \times n}$; K = stiffness matrix, $K \in \Re^{n \times n}$, $q(t)$ = displacement of the n DOF and $f(t)$ = external force vector. Defining $x_1 = q$, and $x_2 = \dot{q}$, Equation (92) can be expressed in the state space representation

$$\begin{bmatrix} \dot{x}_1 \\ \dot{x}_2 \end{bmatrix} = \begin{bmatrix} 0 & I \\ -M^{-1}K & -M^{-1}D \end{bmatrix} \begin{bmatrix} x_1 \\ x_2 \end{bmatrix} + \begin{bmatrix} 0 \\ M^{-1} \end{bmatrix} f \Leftrightarrow \dot{x} = Ax + Bf . \tag{93}$$

The overall structural system matrices M, D and K are the result of the contribution of each structural element; this can be expressed as

$$M = \sum_{i=1}^{e} M^i , \tag{94}$$

$$D = \sum_{i=1}^{e} D^i \tag{95}$$

and

$$K = \sum_{i=1}^{e} K^i , \tag{96}$$

where e is the number of structural elements, and M^i, D^i and K^i are the respective contribution of the i^{th} structural element to the overall system mass, damping and stiffness matrices. The matrices M^i, D^i and K^i can be determined from the finite element model (FEM). For bridge-like structures, the damage affects mainly the stiffness and the damping of the structural members, but not their mass. Therefore, it will be assumed that the mass matrix M does not change due to faults in the structure. Once a structural element has been damaged, its stiffness and/or damping contribution is reduced by a certain amount referred as the reduction factor which can be expressed as

$$D_d = D + \sum_{i=1}^{e} a_i D^i = \sum_{i=1}^{e} (1 + a_i) D^i \tag{97}$$

and

$$K_d = K + \sum_{i=1}^{e} b_i K^i = \sum_{i=1}^{e} (1 + b_i) K^i, \tag{98}$$

where the subscript d corresponds to the damaged structure. The objective of the GDDA is to determine the respective damping and stiffness reduction factors, a_i and b_i.

The state space representation for a damaged structure is

$$\begin{bmatrix} \dot{x}_1 \\ \dot{x}_2 \end{bmatrix} = \begin{bmatrix} 0 & I \\ -M^{-1} \sum_{i=1}^{e} (1 + b_i) K^i & -M^{-1} \sum_{i=1}^{e} (1 + a_i) D^i \end{bmatrix} \begin{bmatrix} x_1 \\ x_2 \end{bmatrix} + \begin{bmatrix} 0 \\ M^{-1} \end{bmatrix} f \Leftrightarrow \tag{99}$$

$$\Leftrightarrow \dot{x}_d = A_d x_d + B_d f. \tag{100}$$

For a particular structural system, matrices A and A_d must be determined using a system identification technique such as the ERA. Subtracting matrix A from matrix A_d:

$$A_d - A = \begin{bmatrix} 0 & 0 \\ -M^{-1}\tilde{K} & -M^{-1}\tilde{D} \end{bmatrix}. \tag{101}$$

The matrix M is known from the FEM for the healthy structure, therefore, the matrices $\tilde{K}$ and $\tilde{D}$ can be extracted using the following equations respectively

$$\tilde{K}_{n\times n} = (-M)(-M^{-1})\tilde{K} = \sum_{i=1}^{e} b_i K^i \tag{102}$$

$$\tilde{D}_{n\times n} = (-M)(-M^{-1})\tilde{D} = \sum_{i=1}^{e} a_i D^i. \tag{103}$$

Equations (102) and (103), can be used to determine the reduction factors a_i and b_i. Expanding Equation (102)

$$\tilde{K} = b_1 K^1 + b_2 K^2 + \ldots + b_e K^e. \tag{104}$$

Equating element by element in Equation (104) and re-arranging in a matrix-vector equation,

$$\begin{bmatrix} \tilde{K}_{11} \\ \cdots \\ \tilde{K}_{1n} \\ \tilde{K}_{21} \\ \cdots \\ \tilde{K}_{2n} \\ \cdots \\ \tilde{K}_{n1} \\ \cdots \\ \tilde{K}_{nn} \end{bmatrix} = \begin{bmatrix} K_{11}^1 & K_{11}^2 & \cdots & K_{11}^e \\ \cdots & \cdots & \cdots & \cdots \\ K_{1n}^1 & K_{1n}^2 & \cdots & K_{1n}^e \\ K_{21}^1 & K_{21}^2 & \cdots & K_{21}^e \\ \cdots & \cdots & \cdots & \cdots \\ K_{2n}^1 & K_{2n}^2 & \cdots & K_{2n}^e \\ \cdots & \cdots & \cdots & \cdots \\ K_{n1}^1 & K_{n1}^2 & \cdots & K_{n1}^e \\ \cdots & \cdots & \cdots & \cdots \\ K_{nn}^1 & K_{nn}^2 & \cdots & K_{nn}^e \end{bmatrix} \begin{bmatrix} b_1 \\ b_2 \\ \cdots \\ b_e \end{bmatrix} \Leftrightarrow \tilde{k} = \widehat{K}\hat{b}, \tag{105}$$

where the subscripts *ij* refer to the element (*i,j*) of the matrix. Note that both matrices $\widehat{K}$ and $\tilde{k}$ will be known. After eliminating the zero-rows of $\widehat{K}$, the resultant matrix is represented as $\widehat{\underset{\sim}{K}}$. The corresponding elements of $\tilde{k}$, which also be equal to zero, are also removed; the resultant vector is represented as $\tilde{\underset{\sim}{k}}$. The stiffness reduction factors, $\hat{b}$, can be determined by

$$\hat{b} = \widehat{\underset{\sim}{K}}^{\dagger}\tilde{\underset{\sim}{k}} \tag{106}$$

where $\widehat{\underset{\sim}{K}}^{\dagger}$ represents the pseudo-inverse of $\widehat{\underset{\sim}{K}}$. A dual development can be done for determining the damping reduction factors $\hat{a}$, so that

$$\begin{bmatrix} \tilde{D}_{11} \\ \cdots \\ \tilde{D}_{1n} \\ \tilde{D}_{21} \\ \cdots \\ \tilde{D}_{2n} \\ \cdots \\ \tilde{D}_{n1} \\ \cdots \\ \tilde{D}_{nn} \end{bmatrix} = \begin{bmatrix} D_{11}^{1} & D_{11}^{2} & \cdots & D_{11}^{e} \\ \cdots & \cdots & \cdots & \cdots \\ D_{1n}^{1} & D_{1n}^{2} & \cdots & D_{1n}^{e} \\ D_{21}^{1} & D_{21}^{2} & \cdots & D_{21}^{e} \\ \cdots & \cdots & \cdots & \cdots \\ D_{2n}^{1} & D_{2n}^{2} & \cdots & D_{2n}^{e} \\ \cdots & \cdots & \cdots & \cdots \\ D_{n1}^{1} & D_{n1}^{2} & \cdots & D_{n1}^{e} \\ \cdots & \cdots & \cdots & \cdots \\ D_{nn}^{1} & D_{nn}^{2} & \cdots & D_{nn}^{e} \end{bmatrix} \begin{bmatrix} a_1 \\ a_2 \\ \cdots \\ a_e \end{bmatrix} \Leftrightarrow \tilde{d} = \widehat{D}\,\grave{b}. \tag{107}$$

After eliminating the zero-rows of $\widehat{D}$, the resultant matrix is represented as $\underset{\sim}{\widehat{D}}$. The corresponding elements of $\tilde{d}$, which also be equal to zero, are also removed; the resultant vector is represented as $\underset{\sim}{\tilde{d}}$. The stiffness reduction factors, $\grave{a}$, can be determined by

$$\grave{a} = \underset{\sim}{\widehat{D}}^{\dagger}\underset{\sim}{\tilde{d}}. \tag{108}$$

Each location in the reduction factor vectors, $\grave{a}$ and $\grave{b}$, corresponds to a particular structural element. Therefore, once the reduction factor vectors have been determined using Equations (106) and (108), the percentage of stiffness and damping reduction for each structural element has been estimated. So that, both the location and severity of the damage are estimated in only one step, contrary to other GDDA, such as the Best Achievable Eigenvector (BAE), in which the possible damage locations are identified first, and then the damage assessment is estimated following a different procedure. Another advantage of the proposed GDDA over the BAE is in

case of multiple damages. The proposed algorithm provides for determining the location and severity of the damage in only one step even when there are multiple damages; while the BAE proposes an iterative process for estimating the different levels of damage.

The proposed algorithm determines the location of the damages and their severity by solving a set of algebraic equations obtained from the state space models of the healthy and damaged structure. Note that the state space representation for the damaged structure is estimated by a system identification method. Certain level of uncertainty is added by the system identification procedure. This uncertainty needs to be considered when interpreting the estimated reduction factors. A small percentage of reduction may result from the deviation of the identified structure with respect to the actual structure.

B. TRANSFORMATION INTO THE PHYSICAL COORDINATE SYSTEM

The proposed damage detection method requires the structural models in the physical coordinate state space representation; in which the first and second half of the state vector, respectively correspond to the displacement and velocity of the structural DOF. Therefore, it is required to linearly transform the identified state space representation into the physical coordinate state space representation of the structure. Note that the identified state space representation contains an arbitrary set of states. Before transforming the identified state space representation it must be in the continuous time domain.

Consider the identified continuous state space representation for an n-DOF damaged structure to have the following state space matrices $A_{d_{id}}$ and $B_{d_{id}}$,

$$A_{d_{id}} = \begin{bmatrix} a_{(1,1)} & \cdots & a_{(1,n)} & a_{(1,n+1)} & \cdots & a_{(1,2n)} \\ \cdots & \cdots & \cdots & \cdots & \cdots & \cdots \\ a_{(n,1)} & \cdots & a_{(n,n)} & a_{(n,n+1)} & \cdots & a_{(n,2n)} \\ a_{(n+1,1)} & \cdots & a_{(n+1,n)} & a_{(n+1,n+1)} & \cdots & a_{(n+1,2n)} \\ \cdots & \cdots & \cdots & \cdots & \cdots & \cdots \\ a_{(2n,1)} & \cdots & a_{(2n,n)} & a_{(2n,n+1)} & \cdots & a_{(2n,2n)} \end{bmatrix}, \tag{109}$$

and

$$B_{d_{id}} = \begin{bmatrix} b_{(1,1)} & \cdots & b_{(1,n)} \\ \cdots & \cdots & \cdots \\ b_{(2n,1)} & \cdots & b_{(2n,n)} \end{bmatrix}. \tag{110}$$

Note that the elements of the matrices $A_{d_{id}}$ and $B_{d_{id}}$ have been denoted without the subscript d for simplicity. Consider the hat on a subscript, $G_{\hat{i}}$, to denote the i^{th} column of the matrix G; and the arrow on a subscript, $G_{\underset{i}{\rightarrow}}$, to denote the i^{th} row of the matrix G. Using these notations the matrices $A_{d_{id}}$ and $B_{d_{id}}$ can be expressed as

$$A_{d_{id}} = \begin{bmatrix} A_{d_{id}\hat{1}} & \cdots & A_{d_{id}\hat{n}} & A_{d_{id}\hat{n+1}} & \cdots & A_{d_{id}\hat{2n}} \end{bmatrix} = \begin{bmatrix} A_{d_{id}\underset{1}{\rightarrow}} \\ \cdots \\ A_{d_{id}\underset{n}{\rightarrow}} \\ A_{d_{id}\underset{n+1}{\longrightarrow}} \\ \cdots \\ A_{d_{id}\underset{2n}{\rightarrow}} \end{bmatrix} \tag{111}$$

and

$$B_{d_{id}} = \begin{bmatrix} B_{d_{id}\rightarrow} \\ \quad 1 \\ \cdots \\ B_{d_{id}\rightarrow} \\ \quad 2n \end{bmatrix}. \tag{112}$$

The objective of the linear transformation is to bring the arbitrary matrices given in Equations (111) and (112) into the physical coordinate system,

$$\begin{bmatrix} \dot{x}_{d_1} \\ \dot{x}_{d_2} \end{bmatrix} = \begin{bmatrix} 0 & I \\ -M^{-1}K_d & -M^{-1}D_d \end{bmatrix} \begin{bmatrix} x_{d_1} \\ x_{d_2} \end{bmatrix} + \begin{bmatrix} 0 \\ M^{-1} \end{bmatrix} f \Leftrightarrow \dot{x}_d = A_{d_{ph}} x_d + B_{d_{ph}} f, \tag{113}$$

where x_{d_1} = displacement of the DOF for the damaged structure and x_{d_2} = velocity of the DOF for the damaged structure. Consider the state space matrix $A_{d_{ph}}$ to be partitioned as

$$A_{d_{ph}} = \begin{bmatrix} 0_{n,\,n} & I_n \\ A_{d_{ph_{21}}} & A_{d_{ph_{22}}} \end{bmatrix}, \tag{114}$$

where $0_{n,\,n}$ represents a zero-matrix with dimensions $n \times n$, and I_n represents an identity matrix of dimensions $n \times n$.

The required linear transformation should satisfy the following set of equations,

$$A_{d_{ph}} = T^{-1} A_{d_{id}} T \tag{115}$$

and

$$B_{d_{ph}} = T^{-1} B_{d_{id}}, \tag{116}$$

where T is the transformation matrix. Equating element by element, Equations (115) and (116) provide enough algebraic equations to solve for the $6n^2$ unknowns, $4n^2$ unknowns in the transformation matrix T and $2n^2$ unknowns in the state space matrix $A_{d_{ph}}$. Considering that the structural mass is not affected by the structural damage, the matrix $B_{d_{ph}}$ is known from the FEM to be

$$B_{d_{ph}} = \begin{bmatrix} 0 \\ M^{-1} \end{bmatrix}; \tag{117}$$

From Equation (116) half of the matrix T elements ($2n^2$ unknowns) can be determined. The rest of the unknowns, $4n^2$, can be determined by solving the algebraic equations obtained using Equation (115).

Consider the linear transformation for a 2-DOF structure, for which $A_{d_{ph}}$, $A_{d_{id}}$, $B_{d_{id}}$, M^{-1} and T, are defined to be

$$A_{d_{ph}} = \begin{bmatrix} 0 & 0 & 1 & 0 \\ 0 & 0 & 0 & 1 \\ a_{d_{ph_{31}}} & a_{d_{ph_{32}}} & a_{d_{ph_{33}}} & a_{d_{ph_{34}}} \\ a_{d_{ph_{41}}} & a_{d_{ph_{42}}} & a_{d_{ph_{43}}} & a_{d_{ph_{44}}} \end{bmatrix}, \tag{118}$$

$$A_{d_{id}} = \begin{bmatrix} a_{11} & a_{12} & a_{13} & a_{14} \\ a_{21} & a_{22} & a_{23} & a_{24} \\ a_{31} & a_{32} & a_{33} & a_{34} \\ a_{41} & a_{42} & a_{43} & a_{44} \end{bmatrix}, \tag{119}$$

$$B_{d_{id}} = \begin{bmatrix} b_{11} & b_{12} \\ b_{21} & b_{22} \\ b_{31} & b_{32} \\ b_{41} & b_{42} \end{bmatrix}, \tag{120}$$

$$M^{-1} = \begin{bmatrix} m_{11} & m_{12} \\ m_{21} & m_{22} \end{bmatrix}^{-1} = \begin{bmatrix} mi_{11} & mi_{12} \\ mi_{21} & mi_{22} \end{bmatrix} \tag{121}$$

and

$$T = \begin{bmatrix} t_{11} & t_{12} & t_{13} & t_{14} \\ t_{21} & t_{22} & t_{23} & t_{24} \\ t_{31} & t_{32} & t_{33} & t_{34} \\ t_{41} & t_{42} & t_{43} & t_{44} \end{bmatrix}. \tag{122}$$

For a 2-DOF Equation (116) comes to be

$$\begin{bmatrix} t_{11} & t_{12} & t_{13} & t_{14} \\ t_{21} & t_{22} & t_{23} & t_{24} \\ t_{31} & t_{32} & t_{33} & t_{34} \\ t_{41} & t_{42} & t_{43} & t_{44} \end{bmatrix} \begin{bmatrix} 0 & 0 \\ 0 & 0 \\ mi_{11} & mi_{12} \\ mi_{21} & mi_{22} \end{bmatrix} = \begin{bmatrix} b_{11} & b_{12} \\ b_{21} & b_{22} \\ b_{31} & b_{32} \\ b_{41} & b_{42} \end{bmatrix}. \tag{123}$$

Expanding Equation (123), and equating element by element

$$\begin{bmatrix} mi_{11} & mi_{21} & & & & & & \\ mi_{12} & mi_{22} & & & & & & \\ & & mi_{11} & mi_{21} & & & & \\ & & mi_{12} & mi_{22} & & & & \\ & & & & mi_{11} & mi_{21} & & \\ & & & & mi_{12} & mi_{22} & & \\ & & & & & & mi_{11} & mi_{21} \\ & & & & & & mi_{12} & mi_{22} \end{bmatrix} \begin{bmatrix} t_{13} \\ t_{14} \\ t_{23} \\ t_{24} \\ t_{33} \\ t_{34} \\ t_{43} \\ t_{44} \end{bmatrix} = \begin{bmatrix} b_{11} \\ b_{12} \\ b_{21} \\ b_{22} \\ b_{31} \\ b_{32} \\ b_{41} \\ b_{42} \end{bmatrix}. \tag{124}$$

In Equation (124) the elements which are equal to zero have been left in blank. Note that Equation (124) contains four decoupled set of equations which can be solved independently:

$$\begin{bmatrix} t_{13} \\ t_{14} \end{bmatrix} = \begin{bmatrix} m_{11} & m_{21} \\ m_{12} & m_{22} \end{bmatrix} \begin{bmatrix} b_{11} \\ b_{12} \end{bmatrix}, \tag{125}$$

$$\begin{bmatrix} t_{23} \\ t_{24} \end{bmatrix} = \begin{bmatrix} m_{11} & m_{21} \\ m_{12} & m_{22} \end{bmatrix} \begin{bmatrix} b_{21} \\ b_{22} \end{bmatrix}, \tag{126}$$

$$\begin{bmatrix} t_{33} \\ t_{34} \end{bmatrix} = \begin{bmatrix} m_{11} & m_{21} \\ m_{12} & m_{22} \end{bmatrix} \begin{bmatrix} b_{31} \\ b_{32} \end{bmatrix} \tag{127}$$

and

$$\begin{bmatrix} t_{43} \\ t_{44} \end{bmatrix} = \begin{bmatrix} m_{11} & m_{21} \\ m_{12} & m_{22} \end{bmatrix} \begin{bmatrix} b_{41} \\ b_{42} \end{bmatrix}. \tag{128}$$

The Equations (125) to (128) can be expressed as

$$\begin{bmatrix} t_{(g,3)} \\ t_{(g,4)} \end{bmatrix} = M^T \begin{bmatrix} b_{(g,1)} \\ b_{(g,2)} \end{bmatrix}, \tag{129}$$

where $g = [1, 2, 3, 4]$. Note that using Equation (129), the last 2 columns of the transformation matrix T are determined. In order to determine the first two columns of the transformation matrix T, Equation (115) must be expanded. Equation (115) can be expressed as

$$TA_{d_{ph}} = A_{d_{id}}T; \tag{130}$$

and for a 2-DOF structure

$$\begin{bmatrix} t_{11} & t_{12} & t_{13} & t_{14} \\ t_{21} & t_{22} & t_{23} & t_{24} \\ t_{31} & t_{32} & t_{33} & t_{34} \\ t_{41} & t_{42} & t_{43} & t_{44} \end{bmatrix} \begin{bmatrix} 0 & 0 & 1 & 0 \\ 0 & 0 & 0 & 1 \\ a_{ph_{31}} & a_{ph_{32}} & a_{ph_{32}} & a_{ph_{34}} \\ a_{ph_{41}} & a_{ph_{42}} & a_{ph_{43}} & a_{ph_{44}} \end{bmatrix} = \tag{131}$$

$$= \begin{bmatrix} a_{11} & a_{12} & a_{13} & a_{14} \\ a_{21} & a_{22} & a_{23} & a_{24} \\ a_{31} & a_{32} & a_{33} & a_{34} \\ a_{41} & a_{42} & a_{43} & a_{44} \end{bmatrix} \begin{bmatrix} t_{11} & t_{12} & t_{13} & t_{14} \\ t_{21} & t_{22} & t_{23} & t_{24} \\ t_{31} & t_{32} & t_{33} & t_{34} \\ t_{41} & t_{42} & t_{43} & t_{44} \end{bmatrix} \tag{132}$$

Expanding Equations (131) and (132), and equating element by element, the following equation is obtained

$$\begin{bmatrix} P_{11} & P_{12} \\ P_{21} & P_{22} \end{bmatrix} \begin{bmatrix} v_1 \\ v_2 \end{bmatrix} = \begin{bmatrix} 0 \\ v_3 \end{bmatrix}, \tag{133}$$

where

$$P_{11} = \begin{bmatrix} a_{11} & 0 & a_{12} & 0 & a_{13} & 0 & a_{14} & 0 \\ a_{21} & 0 & a_{22} & 0 & a_{23} & 0 & a_{24} & 0 \\ a_{31} & 0 & a_{32} & 0 & a_{33} & 0 & a_{34} & 0 \\ a_{41} & 0 & a_{42} & 0 & a_{43} & 0 & a_{44} & 0 \\ 0 & a_{11} & 0 & a_{12} & 0 & a_{13} & 0 & a_{14} \\ 0 & a_{21} & 0 & a_{22} & 0 & a_{23} & 0 & a_{24} \\ 0 & a_{31} & 0 & a_{32} & 0 & a_{33} & 0 & a_{34} \\ 0 & a_{41} & 0 & a_{42} & 0 & a_{43} & 0 & a_{44} \end{bmatrix}, \tag{134}$$

$$P_{12} = \begin{bmatrix} -t_{13} & 0 & 0 & 0 & -t_{14} & 0 & 0 & 0 \\ -t_{23} & 0 & 0 & 0 & -t_{24} & 0 & 0 & 0 \\ -t_{33} & 0 & 0 & 0 & -t_{34} & 0 & 0 & 0 \\ -t_{43} & 0 & 0 & 0 & -t_{44} & 0 & 0 & 0 \\ 0 & -t_{13} & 0 & 0 & 0 & -t_{14} & 0 & 0 \\ 0 & -t_{23} & 0 & 0 & 0 & -t_{24} & 0 & 0 \\ 0 & -t_{33} & 0 & 0 & 0 & -t_{34} & 0 & 0 \\ 0 & -t_{43} & 0 & 0 & 0 & -t_{44} & 0 & 0 \end{bmatrix}, \tag{135}$$

$$P_{21} = I_8, \tag{136}$$

$$P_{22} = \begin{bmatrix} 0 & 0 & t_{13} & 0 & 0 & 0 & t_{14} & 0 \\ 0 & 0 & 0 & t_{13} & 0 & 0 & 0 & t_{14} \\ 0 & 0 & t_{23} & 0 & 0 & 0 & t_{24} & 0 \\ 0 & 0 & 0 & t_{23} & 0 & 0 & 0 & t_{24} \\ 0 & 0 & t_{33} & 0 & 0 & 0 & t_{34} & 0 \\ 0 & 0 & 0 & t_{33} & 0 & 0 & 0 & t_{34} \\ 0 & 0 & t_{43} & 0 & 0 & 0 & t_{44} & 0 \\ 0 & 0 & 0 & t_{43} & 0 & 0 & 0 & t_{44} \end{bmatrix}, \tag{137}$$

$$v_1 = \left[t_{11}\ t_{12}\ t_{21}\ t_{22}\ t_{31}\ t_{32}\ t_{41}\ t_{42}\right]^T, \tag{138}$$

$$v_2 = \left[a_{dph_{31}}\ a_{dph_{32}}\ a_{dph_{33}}\ a_{dph_{34}}\ a_{dph_{41}}\ a_{dph_{42}}\ a_{dph_{43}}\ a_{dph_{44}}\right]^T \tag{139}$$

and

$$v_3 = \left[v_{3_1}\ v_{3_2}\right], \tag{140}$$

where

$$v_{3_1} = \left[A_{did_{\hat{1}}}{}^{T}{}_{\hat{3}}\ \ A_{did_{\hat{1}}}{}^{T}{}_{\hat{4}}\ \ A_{did_{\hat{2}}}{}^{T}{}_{\hat{3}}\ \ A_{did_{\hat{2}}}{}^{T}{}_{\hat{4}}\right] \tag{141}$$

and

$$v_{3_2} = \left[A_{did_{\hat{3}}}{}^{T}{}_{\hat{3}}\ \ A_{did_{\hat{3}}}{}^{T}{}_{\hat{4}}\ \ A_{did_{\hat{4}}}{}^{T}{}_{\hat{3}}\ \ A_{did_{\hat{4}}}{}^{T}{}_{\hat{4}}\right]. \tag{142}$$

Using the introduced notation, Equations (134) and (135) can be expressed as

$$P_{11} = \begin{bmatrix} A_{did_{\hat{1}}} & 0_{4,1} & A_{did_{\hat{2}}} & 0_{4,1} & A_{did_{\hat{3}}} & 0_{4,1} & A_{did_{\hat{4}}} & 0_{4,1} \\ 0_{4,1} & A_{did_{\hat{1}}} & 0_{4,1} & A_{did_{\hat{2}}} & 0_{4,1} & A_{did_{\hat{3}}} & 0_{4,1} & A_{did_{\hat{4}}} \end{bmatrix}_{8\times 8} \tag{143}$$

and

$$P_{12} = \begin{bmatrix} -T_{\hat{1}} & 0_{4,3} & -T_{\hat{2}} & 0_{4,2} & 0_{4,1} \\ 0_{4,1} & -T_{\hat{1}} & 0_{4,3} & -T_{\hat{2}} & 0_{4,2} \end{bmatrix}_{8\times 8}. \tag{144}$$

The matrices P_{11}, P_{12} and P_{22} can be expressed in terms of the Kronecker product[1] as

$$P_{11} = \begin{bmatrix} \left[A_{d_{id_{\hat{1}}}} \otimes I_2\right]^T \\ \left[A_{d_{id_{\hat{2}}}} \otimes I_2\right]^T \\ \left[A_{d_{id_{\hat{3}}}} \otimes I_2\right]^T \\ \left[A_{d_{id_{\hat{4}}}} \otimes I_2\right]^T \end{bmatrix}, \tag{145}$$

$$P_{12} = \begin{bmatrix} \left[-T_{\hat{3}} \otimes \left[I_2 \;\; 0_{2,2}\right]\right]^T \\ \left[-T_{\hat{4}} \otimes \left[I_2 \;\; 0_{2,2}\right]\right]^T \end{bmatrix} \tag{146}$$

and

---

1. Consider the matrices $Q = \begin{bmatrix} q_{11} & q_{12} \\ q_{21} & q_{22} \end{bmatrix}_{2\times 2}$ and $R = \begin{bmatrix} r_{11} & r_{12} & r_{13} \\ r_{21} & r_{22} & r_{23} \end{bmatrix}_{2\times 3}$. The Kronecker product $Q \otimes R$ is defined to be

$$Q \otimes R = \begin{bmatrix} q_{11}R & q_{12}R \\ q_{21}R & q_{22}R \end{bmatrix}_{4\times 6} = \begin{bmatrix} q_{11}r_{11} & q_{11}r_{12} & q_{11}r_{13} & q_{12}r_{11} & q_{12}r_{12} & q_{12}r_{13} \\ q_{11}r_{21} & q_{11}r_{22} & q_{11}r_{23} & q_{12}r_{21} & q_{12}r_{22} & q_{12}r_{23} \\ q_{21}r_{11} & q_{21}r_{12} & q_{21}r_{13} & q_{22}r_{11} & q_{22}r_{12} & q_{22}r_{13} \\ q_{21}r_{21} & q_{21}r_{22} & q_{21}r_{23} & q_{22}r_{21} & q_{22}r_{22} & q_{22}r_{23} \end{bmatrix}$$

$$P_{22} = \begin{bmatrix} 0_{8,2}^{T} \\ [T_{\hat{3}} \otimes I_2]^T \\ 0_{8,2}^{T} \\ [T_{\hat{4}} \otimes I_2]^T \end{bmatrix}^T . \tag{147}$$

From Equation (133), the following set of equations are obtained

$$P_{11}v_1 + P_{12}v_2 = 0 \tag{148}$$

$$P_{21}v_1 + P_{22}v_2 = v_3 . \tag{149}$$

Using Equations (148) and (149), v_1 is find to be

$$v_1 = -P_{11}^{-1}P_{12}(P_{22} - P_{11}^{-1}P_{12})^{-1}v_3 . \tag{150}$$

Once the vector v_1 has been determined using Equation (150), all the elements of the transformation matrix T are known. The last two columns of the transformation matrix T are determined using Equation (129); and the first two columns are determined using Equation (150). Knowing the transformation matrix T, the physical coordinate state space matrix $A_{d_{ph}}$ can be determined using Equation (115).

In order to generalize for the case of an n-DOF structure, let consider the case of a 3-DOF; so that the pattern involved in the linear transformation can be observed from the cases of 2 and 3-DOF. For a 3-DOF structure the matrices $A_{d_{ph}}$, $A_{d_{id}}$, $B_{d_{id}}$, M^{-1} and T are define to be

$$A_{d_{ph}} = \begin{bmatrix} 0 & 0 & 0 & 1 & 0 & 0 \\ 0 & 0 & 0 & 0 & 1 & 0 \\ 0 & 0 & 0 & 0 & 0 & 1 \\ a_{d_{ph_{41}}} & a_{d_{ph_{42}}} & a_{d_{ph_{43}}} & a_{d_{ph_{44}}} & a_{d_{ph_{45}}} & a_{d_{ph_{46}}} \\ a_{d_{ph_{51}}} & a_{d_{ph_{52}}} & a_{d_{ph_{53}}} & a_{d_{ph_{54}}} & a_{d_{ph_{55}}} & a_{d_{ph_{56}}} \\ a_{d_{ph_{61}}} & a_{d_{ph_{62}}} & a_{d_{ph_{63}}} & a_{d_{ph_{64}}} & a_{d_{ph_{65}}} & a_{d_{ph_{66}}} \end{bmatrix}, \tag{151}$$

$$A_{d_{id}} = \begin{bmatrix} a_{11} & a_{12} & a_{13} & a_{14} & a_{15} & a_{16} \\ a_{21} & a_{22} & a_{23} & a_{24} & a_{25} & a_{26} \\ a_{31} & a_{32} & a_{33} & a_{34} & a_{35} & a_{36} \\ a_{41} & a_{42} & a_{43} & a_{44} & a_{45} & a_{46} \\ a_{51} & a_{52} & a_{53} & a_{54} & a_{55} & a_{56} \\ a_{61} & a_{62} & a_{63} & a_{64} & a_{65} & a_{66} \end{bmatrix}, \tag{152}$$

$$B_{d_{id}} = \begin{bmatrix} b_{11} & b_{12} & b_{13} \\ b_{21} & b_{22} & b_{23} \\ b_{31} & b_{32} & b_{33} \\ b_{41} & b_{42} & b_{43} \\ b_{51} & b_{52} & b_{53} \\ b_{61} & b_{62} & b_{63} \end{bmatrix}, \tag{153}$$

$$M^{-1} = \begin{bmatrix} m_{11} & m_{12} & m_{13} \\ m_{21} & m_{22} & m_{23} \\ m_{31} & m_{32} & m_{33} \end{bmatrix}^{-1} = \begin{bmatrix} mi_{11} & mi_{12} & mi_{13} \\ mi_{21} & mi_{22} & mi_{23} \\ mi_{31} & mi_{32} & mi_{33} \end{bmatrix} \tag{154}$$

and

$$T = \begin{bmatrix} t_{11} & t_{12} & t_{13} & t_{14} & t_{15} & t_{16} \\ t_{21} & t_{22} & t_{23} & t_{24} & t_{25} & t_{26} \\ t_{31} & t_{32} & t_{33} & t_{34} & t_{35} & t_{36} \\ t_{41} & t_{42} & t_{43} & t_{44} & t_{45} & t_{46} \\ t_{51} & t_{52} & t_{53} & t_{54} & t_{55} & t_{56} \\ t_{61} & t_{62} & t_{63} & t_{64} & t_{65} & t_{66} \end{bmatrix}. \tag{155}$$

Expanding Equation (116) for a 3-DOF structure

$$\begin{bmatrix} t_{11} & t_{12} & t_{13} & t_{14} & t_{15} & t_{16} \\ t_{21} & t_{22} & t_{23} & t_{24} & t_{25} & t_{26} \\ t_{31} & t_{32} & t_{33} & t_{34} & t_{35} & t_{36} \\ t_{41} & t_{42} & t_{43} & t_{44} & t_{45} & t_{46} \\ t_{51} & t_{52} & t_{53} & t_{54} & t_{55} & t_{56} \\ t_{61} & t_{62} & t_{63} & t_{64} & t_{65} & t_{66} \end{bmatrix} \begin{bmatrix} 0 & 0 & 0 \\ 0 & 0 & 0 \\ 0 & 0 & 0 \\ mi_{11} & mi_{12} & mi_{13} \\ mi_{21} & mi_{22} & mi_{23} \\ mi_{31} & mi_{32} & mi_{33} \end{bmatrix} = \begin{bmatrix} b_{11} & b_{12} & b_{13} \\ b_{21} & b_{22} & b_{23} \\ b_{31} & b_{32} & b_{33} \\ b_{41} & b_{42} & b_{43} \\ b_{51} & b_{52} & b_{53} \\ b_{61} & b_{62} & b_{63} \end{bmatrix}. \tag{156}$$

Expanding Equation (156), and equating element by element also leads to an equation that contains a set of decoupled equations, which are

$$\begin{bmatrix} mi_{11} & mi_{21} & mi_{31} \\ mi_{12} & mi_{22} & mi_{32} \\ mi_{13} & mi_{23} & mi_{33} \end{bmatrix} \begin{bmatrix} t_{14} \\ t_{15} \\ t_{16} \end{bmatrix} = \begin{bmatrix} b_{11} \\ b_{12} \\ b_{13} \end{bmatrix}, \tag{157}$$

$$\begin{bmatrix} mi_{11} & mi_{21} & mi_{31} \\ mi_{12} & mi_{22} & mi_{32} \\ mi_{13} & mi_{23} & mi_{33} \end{bmatrix} \begin{bmatrix} t_{24} \\ t_{25} \\ t_{26} \end{bmatrix} = \begin{bmatrix} b_{21} \\ b_{22} \\ b_{23} \end{bmatrix}, \tag{158}$$

$$\begin{bmatrix} mi_{11} & mi_{21} & mi_{31} \\ mi_{12} & mi_{22} & mi_{32} \\ mi_{13} & mi_{23} & mi_{33} \end{bmatrix} \begin{bmatrix} t_{34} \\ t_{35} \\ t_{36} \end{bmatrix} = \begin{bmatrix} b_{31} \\ b_{32} \\ b_{33} \end{bmatrix}, \tag{159}$$

$$\begin{bmatrix} mi_{11} & mi_{21} & mi_{31} \\ mi_{12} & mi_{22} & mi_{32} \\ mi_{13} & mi_{23} & mi_{33} \end{bmatrix} \begin{bmatrix} t_{44} \\ t_{45} \\ t_{46} \end{bmatrix} = \begin{bmatrix} b_{41} \\ b_{42} \\ b_{43} \end{bmatrix}, \tag{160}$$

$$\begin{bmatrix} mi_{11} & mi_{21} & mi_{31} \\ mi_{12} & mi_{22} & mi_{32} \\ mi_{13} & mi_{23} & mi_{33} \end{bmatrix} \begin{bmatrix} t_{54} \\ t_{55} \\ t_{56} \end{bmatrix} = \begin{bmatrix} b_{51} \\ b_{52} \\ b_{53} \end{bmatrix} \tag{161}$$

and

$$\begin{bmatrix} mi_{11} & mi_{21} & mi_{31} \\ mi_{12} & mi_{22} & mi_{32} \\ mi_{13} & mi_{23} & mi_{33} \end{bmatrix} \begin{bmatrix} t_{64} \\ t_{65} \\ t_{66} \end{bmatrix} = \begin{bmatrix} b_{61} \\ b_{62} \\ b_{63} \end{bmatrix}. \tag{162}$$

The Equations (157) to (162) can all be solved as

$$\begin{bmatrix} t_{(g,4)} \\ t_{(g,5)} \\ t_{(g,6)} \end{bmatrix} = M^T \begin{bmatrix} b_{(g,1)} \\ b_{(g,2)} \\ b_{(g,3)} \end{bmatrix}, \tag{163}$$

where $g = [1, 2, \ldots, 6]$. Note that using Equation (163) the last 3 columns of the transformation matrix T are determined. In order to determine the first 3 columns of the transformation matrix T, Equation (115) must be expanded. Equation (115) can be expressed as Equation (130); and for a 3-DOF this comes to be

$$\begin{bmatrix} t_{11} & t_{12} & t_{13} & t_{14} & t_{15} & t_{16} \\ t_{21} & t_{22} & t_{23} & t_{24} & t_{25} & t_{26} \\ t_{31} & t_{32} & t_{33} & t_{34} & t_{35} & t_{36} \\ t_{41} & t_{42} & t_{43} & t_{44} & t_{45} & t_{46} \\ t_{51} & t_{52} & t_{53} & t_{54} & t_{55} & t_{56} \\ t_{61} & t_{62} & t_{63} & t_{64} & t_{65} & t_{66} \end{bmatrix} \begin{bmatrix} 0 & 0 & 0 & 1 & 0 & 0 \\ 0 & 0 & 0 & 0 & 1 & 0 \\ 0 & 0 & 0 & 0 & 0 & 1 \\ a_{ph_{41}} & a_{ph_{42}} & a_{ph_{43}} & a_{ph_{44}} & a_{ph_{45}} & a_{ph_{46}} \\ a_{ph_{51}} & a_{ph_{52}} & a_{ph_{53}} & a_{ph_{54}} & a_{ph_{55}} & a_{ph_{56}} \\ a_{ph_{61}} & a_{ph_{62}} & a_{ph_{63}} & a_{ph_{64}} & a_{ph_{65}} & a_{ph_{66}} \end{bmatrix} = \tag{164}$$

$$= \begin{bmatrix} a_{11} & a_{12} & a_{13} & a_{14} & a_{15} & a_{16} \\ a_{21} & a_{22} & a_{23} & a_{24} & a_{25} & a_{26} \\ a_{31} & a_{32} & a_{33} & a_{34} & a_{35} & a_{36} \\ a_{41} & a_{42} & a_{43} & a_{44} & a_{45} & a_{46} \\ a_{51} & a_{52} & a_{53} & a_{54} & a_{55} & a_{56} \\ a_{61} & a_{62} & a_{63} & a_{64} & a_{65} & a_{66} \end{bmatrix} \begin{bmatrix} t_{11} & t_{12} & t_{13} & t_{14} & t_{15} & t_{16} \\ t_{21} & t_{22} & t_{23} & t_{24} & t_{25} & t_{26} \\ t_{31} & t_{32} & t_{33} & t_{34} & t_{35} & t_{36} \\ t_{41} & t_{42} & t_{43} & t_{44} & t_{45} & t_{46} \\ t_{51} & t_{52} & t_{53} & t_{54} & t_{55} & t_{56} \\ t_{61} & t_{62} & t_{63} & t_{64} & t_{65} & t_{66} \end{bmatrix}. \tag{165}$$

Expanding Equations (164) and (165), and equating element by element also leads to Equation (133), where

$$P_{11} = \begin{bmatrix} P_{11_1} & P_{11_2} \end{bmatrix} \tag{166}$$

where

$$P_{11_1} = \begin{bmatrix} A_{id_{\hat{1}}} & 0_{6,2} & A_{id_{\hat{2}}} & 0_{6,2} & A_{id_{\hat{3}}} & 0_{6,1} & 0_{6,1} \\ 0_{6,1} & A_{id_{\hat{1}}} & 0_{6,2} & A_{id_{\hat{2}}} & 0_{6,2} & A_{id_{\hat{3}}} & 0_{6,1} \\ 0_{6,1} & 0_{6,1} & A_{id_{\hat{1}}} & 0_{6,2} & A_{id_{\hat{2}}} & 0_{6,2} & A_{id_{\hat{3}}} \end{bmatrix} \tag{167}$$

and

$$P_{11_2} = \begin{bmatrix} A_{id_{\hat{4}}} & 0_{6,2} & A_{id_{\hat{5}}} & 0_{6,2} & A_{id_{\hat{6}}} & 0_{6,1} & 0_{6,1} \\ 0_{6,1} & A_{id_{\hat{4}}} & 0_{6,2} & A_{id_{\hat{5}}} & 0_{6,2} & A_{id_{\hat{6}}} & 0_{6,1} \\ 0_{6,1} & 0_{6,1} & A_{id_{\hat{4}}} & 0_{6,2} & A_{id_{\hat{5}}} & 0_{6,2} & A_{id_{\hat{6}}} \end{bmatrix}; \tag{168}$$

$$P_{12} = \begin{bmatrix} -T_{\hat{4}} & 0_{6,5} & -T_{\hat{5}} & 0_{6,5} & -T_{\hat{6}} & 0_{6,4} & 0_{6,1} \\ 0_{6,1} & -T_{\hat{4}} & 0_{6,5} & -T_{\hat{5}} & 0_{6,5} & -T_{\hat{6}} & 0_{6,4} \\ 0_{6,2} & -T_{\hat{4}} & 0_{6,5} & -T_{\hat{5}} & 0_{6,5} & -T_{\hat{6}} & 0_{6,3} \end{bmatrix}, \tag{169}$$

$$P_{21} = I_{18}, \tag{170}$$

$$P_{22} = \begin{bmatrix} 0_{3,3} & t_{14}I_3 & 0_{3,3} & t_{15}I_3 & 0_{3,3} & t_{16}I_3 \\ 0_{3,3} & t_{24}I_3 & 0_{3,3} & t_{25}I_3 & 0_{3,3} & t_{26}I_3 \\ 0_{3,3} & t_{34}I_3 & 0_{3,3} & t_{35}I_3 & 0_{3,3} & t_{36}I_3 \\ 0_{3,3} & t_{44}I_3 & 0_{3,3} & t_{45}I_3 & 0_{3,3} & t_{46}I_3 \\ 0_{3,3} & t_{54}I_3 & 0_{3,3} & t_{55}I_3 & 0_{3,3} & t_{56}I_3 \\ 0_{3,3} & t_{64}I_3 & 0_{3,3} & t_{65}I_3 & 0_{3,3} & t_{66}I_3 \end{bmatrix}, \tag{171}$$

$$v_1 = \begin{bmatrix} t_{11} & t_{12} & t_{13} & t_{21} & t_{22} & t_{23} & t_{31} & t_{32} & t_{33} & t_{41} & t_{42} & t_{43} & t_{51} & t_{52} & t_{53} & t_{61} & t_{62} & t_{63} \end{bmatrix}^T, \tag{172}$$

$$v_2 = \begin{bmatrix} A_{d_{ph_{\hat{4}}}} & A_{d_{ph_{\hat{5}}}} & A_{d_{ph_{\hat{6}}}} \end{bmatrix}^T \tag{173}$$

and

$$v_3 = \begin{bmatrix} v_{3_1} & v_{3_2} & v_{3_3} \end{bmatrix}^T, \tag{174}$$

where

$$v_{3_1} = \left[A_{d_{id_{\underset{1}{\rightarrow}}}} T_{\hat{4}} \; A_{d_{id_{\underset{1}{\rightarrow}}}} T_{\hat{5}} \; A_{d_{id_{\underset{1}{\rightarrow}}}} T_{\hat{6}} \; A_{d_{id_{\underset{2}{\rightarrow}}}} T_{\hat{4}} \; A_{d_{id_{\underset{2}{\rightarrow}}}} T_{\hat{5}} \; A_{d_{id_{\underset{2}{\rightarrow}}}} T_{\hat{6}} \right], \tag{175}$$

$$v_{3_2} = \left[A_{d_{id_{\underset{3}{\rightarrow}}}} T_{\hat{4}} \; A_{d_{id_{\underset{3}{\rightarrow}}}} T_{\hat{5}} \; A_{d_{id_{\underset{3}{\rightarrow}}}} T_{\hat{6}} \; A_{d_{id_{\underset{4}{\rightarrow}}}} T_{\hat{4}} \; A_{d_{id_{\underset{4}{\rightarrow}}}} T_{\hat{5}} \; A_{d_{id_{\underset{4}{\rightarrow}}}} T_{\hat{6}} \right] \tag{176}$$

and

$$v_{3_3} = \left[A_{d_{id_{\underset{5}{\rightarrow}}}} T_{\hat{4}} \; A_{d_{id_{\underset{5}{\rightarrow}}}} T_{\hat{5}} \; A_{d_{id_{\underset{5}{\rightarrow}}}} T_{\hat{6}} \; A_{d_{id_{\underset{6}{\rightarrow}}}} T_{\hat{4}} \; A_{d_{id_{\underset{6}{\rightarrow}}}} T_{\hat{5}} \; A_{d_{id_{\underset{6}{\rightarrow}}}} T_{\hat{6}} \right]. \tag{177}$$

The matrices P_{11}, P_{12} and P_{22} can be expressed in terms of the Kronecker product as

$$P_{11} = \begin{bmatrix} \left[A_{d_{id_{\hat{1}}}} \otimes I_3 \right]^T \\ \left[A_{d_{id_{\hat{2}}}} \otimes I_3 \right]^T \\ \left[A_{d_{id_{\hat{3}}}} \otimes I_3 \right]^T \\ \left[A_{d_{id_{\hat{4}}}} \otimes I_3 \right]^T \\ \left[A_{d_{id_{\hat{5}}}} \otimes I_3 \right]^T \\ \left[A_{d_{id_{\hat{6}}}} \otimes I_3 \right]^T \end{bmatrix}^T, \tag{178}$$

$$P_{12} = \begin{bmatrix} \left[-T_{\hat{4}} \otimes \left[I_3 \; 0_{3,3}\right]\right]^T \\ \left[-T_{\hat{5}} \otimes \left[I_3 \; 0_{3,3}\right]\right]^T \\ \left[-T_{\hat{6}} \otimes \left[I_3 \; 0_{3,3}\right]\right]^T \end{bmatrix}^T \tag{179}$$

and

$$P_{22} = \begin{bmatrix} 0_{18,3}^T \\ [T_{\hat{4}} \otimes I_3]^T \\ 0_{18,3}^T \\ [T_{\hat{5}} \otimes I_3]^T \\ 0_{18,3}^T \\ [T_{\hat{6}} \otimes I_3]^T \end{bmatrix}^T . \tag{180}$$

After assembling these matrices, the vector v_1 can be determined using Equation (150). Once the vector v_1 has been determined using Equation (150), all the elements of the transformation matrix T are known. The last three columns of the transformation matrix T are determined using Equation (129); and the first three columns are determined using Equation (150). Knowing the transformation matrix T, the physical coordinate state space matrix $A_{d_{ph}}$ can be determined using Equation (115).

The cases of 2 and 3-DOF have been considered. Let us observe this cases, and based on the obtained results generalize the linear transformation method for an n-DOF. For an n-DOF structure, the matrices $A_{d_{id}}$ and $B_{d_{id}}$ are respectively defined as

in Equations (109) and (110); and the matrices M^{-1}, $\begin{bmatrix} A_{dph_{21}} & A_{dph_{22}} \end{bmatrix}$ and are define to be

$$M^{-1} = \begin{bmatrix} m_{(1,1)} & \cdots & m_{(1,n)} \\ \cdots & \cdots & \cdots \\ m_{(n,1)} & \cdots & m_{(n,n)} \end{bmatrix}^{-1} = \begin{bmatrix} mi_{(1,1)} & \cdots & mi_{(1,n)} \\ \cdots & \cdots & \cdots \\ mi_{(n,1)} & \cdots & mi_{(n,n)} \end{bmatrix}, \tag{181}$$

$$\begin{bmatrix} A_{dph_{21}} & A_{dph_{22}} \end{bmatrix} = \begin{bmatrix} A_{dph_{\substack{\longrightarrow \\ n+1}}} \\ \cdots \\ A_{dph_{\substack{\rightarrow \\ 2n}}} \end{bmatrix} \tag{182}$$

and

$$T = \begin{bmatrix} t_{(1,1)} & \cdots & t_{(1,n)} & t_{(1,n+1)} & \cdots & t_{(1,2n)} \\ \cdots & \cdots & \cdots & \cdots & \cdots & \cdots \\ t_{(n,1)} & \cdots & t_{(n,n)} & t_{(n,n+1)} & \cdots & t_{(n,2n)} \\ t_{(n+1,1)} & \cdots & t_{(n+1,n)} & t_{(n+1,n+1)} & \cdots & t_{(n+1,2n)} \\ \cdots & \cdots & \cdots & \cdots & \cdots & \cdots \\ t_{(2n,1)} & \cdots & t_{(2n,n)} & t_{(2n,n+1)} & \cdots & t_{(2n,2n)} \end{bmatrix}. \tag{183}$$

Observing Equation (129) and (163), which respectively correspond to a 2 and 3-DOF structure, it can be generalized that for an n-DOF

$$\begin{bmatrix} t_{(g,n+1)} \\ \cdots \\ t_{(g,2n)} \end{bmatrix} = M^T \begin{bmatrix} b_{(g,1)} \\ \cdots \\ b_{(g,n)} \end{bmatrix}, \tag{184}$$

where $g = [1, 2, \ldots, 2n]$. Equation (184) allows to determine the last n columns of the transformation matrix T. Considering the presented cases for 2 and 3-DOF, it can be generalized that Equation (115) leads to the equation

$$\begin{bmatrix} P_{11} & P_{12} \\ P_{21} & P_{22} \end{bmatrix} \begin{bmatrix} v_1 \\ v_2 \end{bmatrix} = \begin{bmatrix} 0 \\ v_3 \end{bmatrix}, \tag{185}$$

where P_{21} is an identity matrix of order $2n^2$. From Equation (185) the following equations are obtained

$$v_1 = -P_{11}^{-1} P_{12} v_2 \tag{186}$$

$$v_2 = (P_{22} - P_{11}^{-1} P_{12})^{-1} v_3 . \tag{187}$$

From Equations (186) and (187), the vector v_1 is determined to be

$$v_1 = -P_{11}^{-1} P_{12} (P_{22} - P_{11}^{-1} P_{12})^{-1} v_3 . \tag{188}$$

In Equation (188), the matrices P_{11}, P_{12} and P_{22}, as well as the vectors v_1, v_2 and v_3, depend on the number of degrees of freedom. Based on the cases of 2 and 3 -DOF, these matrices and vectors can be generalized for the case of n-DOF. The vector v_1 contains the elements of the first n columns of the transformation matrix T,

$$v_1 = \left[t_{(1,1)} \cdots t_{(1,n)} \; t_{(2,1)} \cdots t_{(2,n)} \cdots t_{(2n,1)} \cdots t_{(2n,n)} \right]^T . \tag{189}$$

The vector v_2 contains the unknowns elements of the state space matrix $A_{d_{ph}}$,

$$v_2 = \left[A_{ph_{\underset{n+1}{\longrightarrow}}} \; A_{ph_{\underset{n+2}{\longrightarrow}}} \; \cdots \; A_{ph_{\underset{2n}{\rightarrow}}} \right]^T \tag{190}$$

Once Equation (116) has been solve using Equation (184), the vector v_3 is a known quantity,

$$v_3 = \begin{bmatrix} A_{did_{\hat{1}}}{}^T{}_{n\hat{+}1} \\ \cdots \\ A_{did_{\hat{1}}}{}^T{}_{\hat{2n}} \\ A_{did_{\hat{2}}}{}^T{}_{n\hat{+}1} \\ \cdots \\ A_{did_{\hat{2}}}{}^T{}_{\hat{2n}} \\ \cdots \\ A_{did_{\hat{2n}}}{}^T{}_{n\hat{+}1} \\ \cdots \\ A_{did_{\hat{2n}}}{}^T{}_{\hat{2n}} \end{bmatrix}. \tag{191}$$

Based on the results obtained for the 2 and 3-DOF, the matrices P_{11}, P_{12} and P_{22} for an n-DOF can be expressed in terms of the Kronecker product,

$$P_{11} = \begin{bmatrix} \left[A_{did_{\hat{1}}} \otimes I_n\right]^T \\ \left[A_{did_{\hat{2}}} \otimes I_n\right]^T \\ \cdots \\ \left[A_{did_{\hat{n}}} \otimes I_n\right]^T \end{bmatrix}_{2n^2 \times 2n^2}, \tag{192}$$

$$P_{12} = \begin{bmatrix} \left[-T_{n\hat{+}1} \otimes \left[I_n \; 0_{n,n}\right]\right]^T \\ \left[-T_{n\hat{+}2} \otimes \left[I_n \; 0_{n,n}\right]\right]^T \\ \cdots \\ \left[-T_{\hat{2n}} \otimes \left[I_n \; 0_{n,n}\right]\right]^T \end{bmatrix}_{2n^2 \times 2n^2} \tag{193}$$

and

$$P_{22} = \begin{bmatrix} 0^T_{2n^2,n} \\ [T_{n\hat{+}1} \otimes I_n]^T \\ 0^T_{2n^2,n} \\ [T_{n\hat{+}2} \otimes I_n]^T \\ \cdots \\ 0^T_{2n^2,n} \\ [T_{\hat{2n}} \otimes I_n]^T \end{bmatrix}_{2n^2 \times 2n^2} \tag{194}$$

Once the vector v_1 has been determined using Equation (188) all the elements of the transformation matrix T are known. The last n columns of the transformation matrix T are determined using Equation (184); and the first three columns are determined using Equation (188). Knowing the transformation matrix T, the physical coordinate state space matrix $A_{d_{ph}}$ can be determined using Equation (115).

C. LIMITATION IMPOSED BY PROPOSED LINEAR TRANSFORMATION

The proposed linear transformation for getting any arbitrary state space representation into the physical coordinates requires the state space matrix B to have

rank equal to the number of DOF. This limits the application of the linear transformation method to the cases in which there are as many actuators as DOF.

When a state space representation is linearly transform, it does not only affect the state space matrices A_d and B_d; it also affects the state space matrix C_d. The matrix C_d is related to the measurements of the states,

$$y_d = C_d x_d, \tag{195}$$

where y is the vector of measurements. It was felt that using Equation (195), may lead to overcoming the limitation imposed by the proposed linear transformation procedure. The relationship between the arbitrary representation and the physical coordinate is given by

$$C_{d_{ph}} = C_{d_{id}} T. \tag{196}$$

Assuming the displacement of the DOF could be measured, the matrix $C_{d_{ph}}$ is

$$C_{d_{ph}} = \left[I_n \; 0_{n,n} \right]. \tag{197}$$

Expanding Equation (196) for a 3-DOF, and considering $C_{d_{ph}}$ to be

$$C_{d_{ph}} = \left[I_3 \; 0_{3,3} \right], \tag{198}$$

leads to the equation

$$\begin{bmatrix} I_6 \otimes C_{d_{id_{\rightarrow 1}}} \\ I_6 \otimes C_{d_{id_{\rightarrow 2}}} \\ I_6 \otimes C_{d_{id_{\rightarrow 3}}} \end{bmatrix}_{18\times 36} \begin{bmatrix} T_{\hat{1}} \\ T_{\hat{2}} \\ T_{\hat{3}} \\ T_{\hat{4}} \\ T_{\hat{5}} \\ T_{\hat{6}} \end{bmatrix}_{36\times 1} = \begin{bmatrix} C^T_{d_{ph_{\rightarrow 1}}} \\ C^T_{d_{ph_{\rightarrow 2}}} \\ C^T_{d_{ph_{\rightarrow 3}}} \end{bmatrix}_{18\times 1} . \tag{199}$$

Note that in Equation (199) all the elements of the transformation matrix are the unknowns; i.e., there are $4n^2$ unknowns. Considering the base case scenario, in which all the DOF are available for measurement, Equation (196) will provide $2n^2$ equations. Therefore, considering the best measurement scenario, $2n^2$ extra equations are needed in order to solve for all of the unknowns. The other two sources of equations are Equations (115) and (116). If Equation (115) is to be expanded, the last n columns of the transformation matrix T should be known in order to avoid the multiplication of two unknowns. Therefore, the only remaining source of equations is Equation (116), which may add up to $2np_i$ equations; where p_i is the number of inputs. Therefore, in order to obtain the number of equations that were missing under the best measurement scenario (which were $2n^2$), p_i must be equal to n. This shows that, even when all DOF were available for measurement, the required number of actuators remains n. So that, the additional information obtained from Equation (196) does help to overcome the limitation imposed by the proposed procedure for linearly transforming an arbitrary state representation into the physical coordinates.

V. APPLICATION OF THE SATE SPACE BASED GDDA

In this section, a 3-DOF system is used to illustrate step-by-step the proposed global damage detection algorithm (GDDA). Additionally, the obtained results on a simulated three-bar truss structure with 3-DOF are presented, providing the step-by-step procedure for one damage case scenario. The three-bar truss structure was simulated in order to get the structural response to a sequence of random inputs. From the time-domain collected data the state space representation of the structure is obtained applying several system identification methods. Estimating the state space representation of the structure arises the need for using the proposed linear transformation into the physical coordinate of the structure. For both systems, the FEM model will be provided in order to apply the proposed GDDA.

A. Three-DOF System

Consider an undamaged spring-damper-mass 3-DOF system to be as shown in Figure 6, and the damaged system as shown in Figure 7.

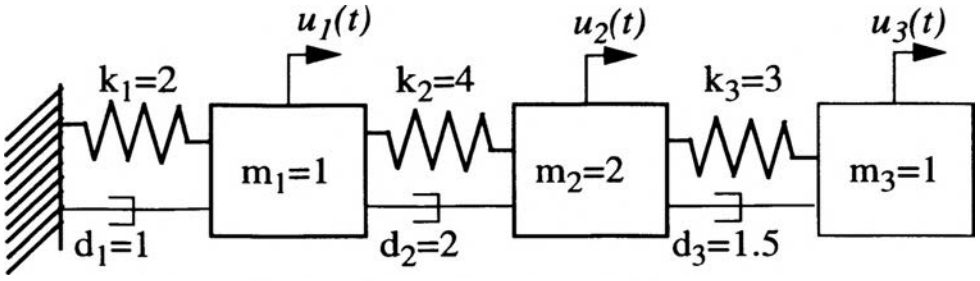

Figure 6. Undamaged 3-DOF system

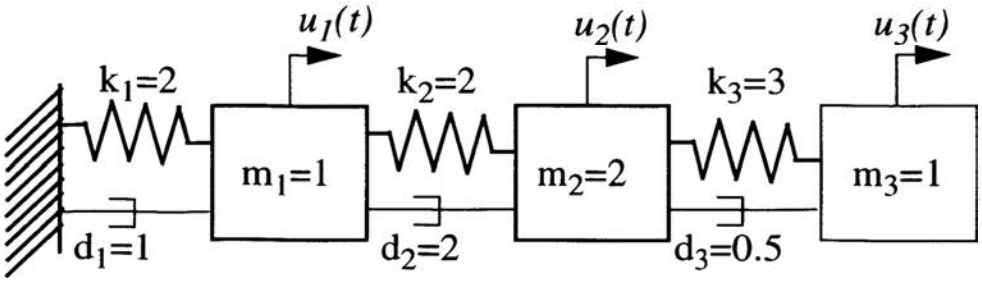

Figure 7. Damaged 3-DOF system

The equation of motion for this 3-DOF system is determined to be

$$\begin{bmatrix} m_1 & 0 & 0 \\ 0 & m_2 & 0 \\ 0 & 0 & m_3 \end{bmatrix} \ddot{q} + \begin{bmatrix} d_1+d_2 & -d_2 & 0 \\ -d_2 & d_2+d_3 & -d_3 \\ 0 & -d_3 & d_3 \end{bmatrix} \dot{q} + \begin{bmatrix} k_1+k_2 & -k_2 & 0 \\ -k_2 & k_2+k_3 & -k_3 \\ 0 & -k_3 & k_3 \end{bmatrix} q = \begin{bmatrix} u_1 \\ u_2 \\ u_3 \end{bmatrix}. \quad (200)$$

Therefore, the matrices A and A_d of the respective state space representation for these systems are:

$$A = \begin{bmatrix} 0 & 0 & 0 & 1 & 0 & 0 \\ 0 & 0 & 0 & 0 & 1 & 0 \\ 0 & 0 & 0 & 0 & 0 & 1 \\ -6 & 4 & 0 & -3 & 2 & 0 \\ 2 & -3.5 & 1.5 & 1 & -1.75 & 0.75 \\ 0 & 3 & -3 & 0 & 1.5 & -1.5 \end{bmatrix} \quad (201)$$

and

$$A_d = \begin{bmatrix} 0 & 0 & 0 & 1 & 0 & 0 \\ 0 & 0 & 0 & 0 & 1 & 0 \\ 0 & 0 & 0 & 0 & 0 & 1 \\ -4 & 2 & 0 & -3 & 2 & 0 \\ 1 & -2.5 & 1.5 & 1 & -1.25 & 0.25 \\ 0 & 3 & -3 & 0 & 0.5 & -0.5 \end{bmatrix}. \quad (202)$$

The eigenvalues, their damping and natural frequencies for the matrices A and A_d are provided in Tables VI and VII, respectively. The damage in the structure causes it to behave differently than the healthy structure; Figure 8 shows the difference of the system singular values.

Table VI: Eigenvalues of matrix A

Eigenvalues	Damping	Freq. (rad/sec)
$-0.0922 \pm j0.6$	0.152	0.607
$-1 \pm j1.732$	0.5	2
$-2.033 \pm j2$	0.713	2.852

Table VII: Eigenvalues of matrix A_d

Eigenvalues	Damping	Freq. (rad/sec)
$-0.102 \pm j0.54$	0.186	0.55
$-0.418 \pm j2.02$	0.2025	2.062
$-1.855 \pm j1.11$	0.8585	2.16

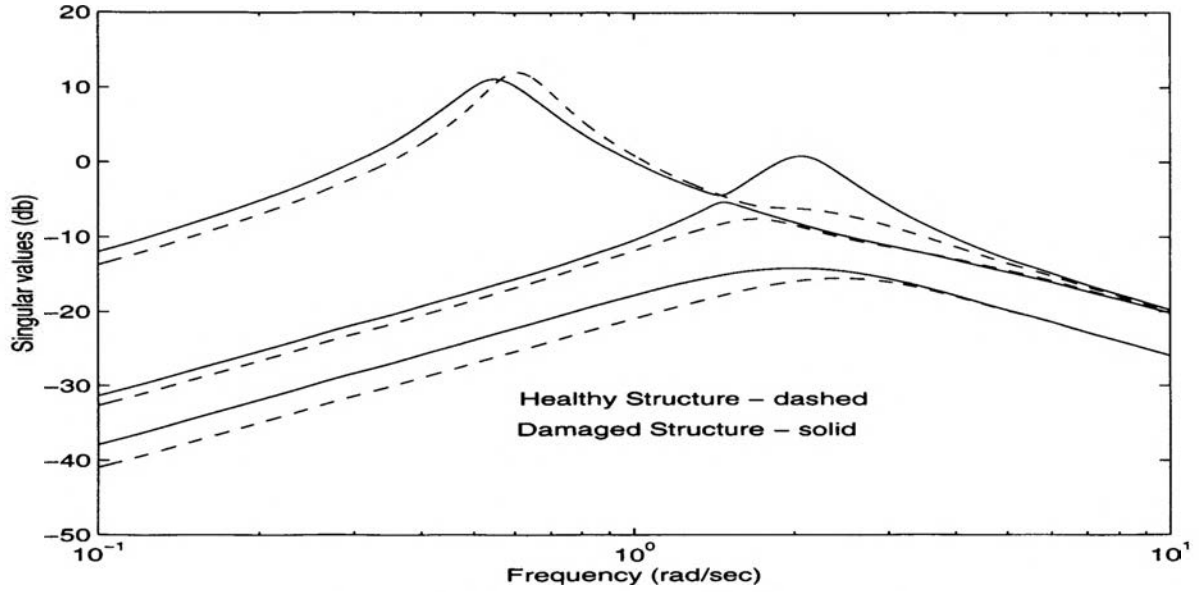

Figure 8. Singular values for 3-DOF structure

Observing the stiffness and damping parameters from Figures 6 and 7, and using Equation (200), the matrices K, D, K_d and D_d for the healthy and damaged structure are determined to be

$$K = \begin{bmatrix} 6 & -4 & 0 \\ -4 & 7 & -3 \\ 0 & -3 & 3 \end{bmatrix}, \tag{203}$$

$$D = \begin{bmatrix} 3 & -2 & 0 \\ -2 & 3.5 & -1.5 \\ 0 & -1.5 & 1.5 \end{bmatrix}, \tag{204}$$

$$K_d = \begin{bmatrix} 4 & -2 & 0 \\ -2 & 5 & -3 \\ 0 & -3 & 3 \end{bmatrix} \tag{205}$$

and

$$D_d = \begin{bmatrix} 3 & -2 & 0 \\ -2 & 2.5 & -0.5 \\ 0 & -0.5 & 0.5 \end{bmatrix} \tag{206}$$

Substracting A from A_d, and determining $\tilde{K}$ and $\tilde{D}$ as respectively shown in Equations (102) and (103),

$$\tilde{K} = \begin{bmatrix} -2 & 2 & 0 \\ 2 & -2 & 0 \\ 0 & 0 & 0 \end{bmatrix} \tag{207}$$

and

$$\tilde{D} = \begin{bmatrix} 0 & 0 & 0 \\ 0 & -1 & 1 \\ 0 & 1 & -1 \end{bmatrix}. \tag{208}$$

Using Equations (106) and (108), the following equations for calculating the damping and stiffness reduction factors, a_i and b_i respectively, are determined to be

$$\begin{bmatrix} 1 & 2 & 0 \\ 0 & -2 & 0 \\ 0 & -2 & 0 \\ 0 & 2 & 1.5 \\ 0 & 0 & -1.5 \\ 0 & 0 & -1.5 \\ 0 & 0 & 1.5 \end{bmatrix} \begin{bmatrix} a_1 \\ a_2 \\ a_3 \end{bmatrix} = \begin{bmatrix} 0 \\ 0 \\ 0 \\ -1 \\ 1 \\ 1 \\ -1 \end{bmatrix} \tag{209}$$

and

$$\begin{bmatrix} 2 & 4 & 0 \\ 0 & -4 & 0 \\ 0 & -4 & 0 \\ 0 & 4 & 3 \\ 0 & 0 & -3 \\ 0 & 0 & -3 \\ 0 & 0 & 3 \end{bmatrix} \begin{bmatrix} b_1 \\ b_2 \\ b_3 \end{bmatrix} = \begin{bmatrix} -2 \\ 2 \\ 2 \\ -2 \\ 0 \\ 0 \\ 0 \end{bmatrix}. \tag{210}$$

Using the pseudoinverse of the matrices, the following results are obtained,

$$\begin{bmatrix} b_1 \\ b_2 \\ b_3 \end{bmatrix} = \begin{bmatrix} 0 \\ -0.5 \\ 0 \end{bmatrix} \text{ and } \begin{bmatrix} a_1 \\ a_2 \\ a_3 \end{bmatrix} = \begin{bmatrix} 0 \\ 0 \\ -0.667 \end{bmatrix}. \tag{211}$$

From these results, it can be seen that both reduction factors b_2 and a_3 have been properly identified. These values indicate a 50% reduction in the stiffness of the spring number 2, which connects the 1st and 2nd masses, as well as a 66.7% reduction in the damping of the damper number 3, which connects the 2nd and 3rd masses. Note that both the location and extent of the damages were determined at the same time.

B. Simulated Three-bar 3-DOF Structure

The three-bar 3-DOF structure shown in Figure 9 was simulated in order to get the input-output data for the structure. The DOF are represented by the arrows, which at the same time indicate the location for the actuators. The mass, stiffness and damping parameters for the structure are given in Table VIII, where the values for the healthy structure as well as for the different damage scenarios considered are provided. The constants k_i and d_i, respectively, represent the stiffness and damping

parameters for the i^{th} element of the structure, as numbered in Figure 9. Note that the damage scenario 4 is the combination of the damage scenarios 1, 2 and 3.

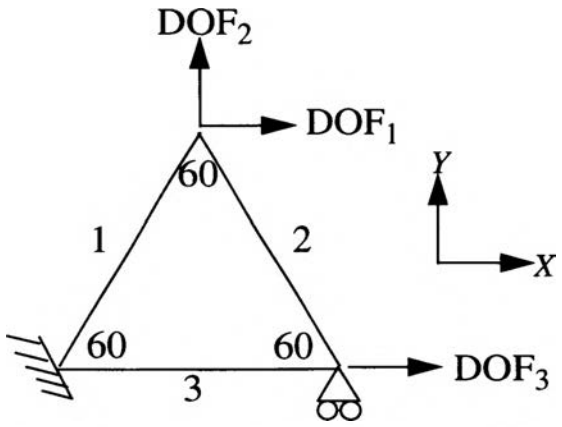

Figure 9. Simulated three-bar 3-DOF structure

Table VIII: Structural parameters for the three-bar 3 DOF structure

structure	$m_{1,2,3}$	k_1	k_2	k_3	d_1	d_2	d_3
healthy	4	7	7	7	6	6	6
damage 1	4	2.45	7	7	6	1.5	6
damage 2	4	7	3.85	7	4.2	6	6
damage 3	4	7	7	3.15	6	6	3.75
damage 4	4	2.45	3.85	3.15	4.2	1.5	3.75

Two different procedure were used to perform the system identification for the damage scenario 1. The first procedure was to use the ERA algorithm to estimate the

state space representation for the structure based on the estimated Markov parameters by a feedforward neural network. The second procedure was to use the *System Identification Toolbox of MATLAB* to identify the state space representation of the structure.

The nominal difference in the singular values of the system under the damage scenario 1 is shown in Figure 10.

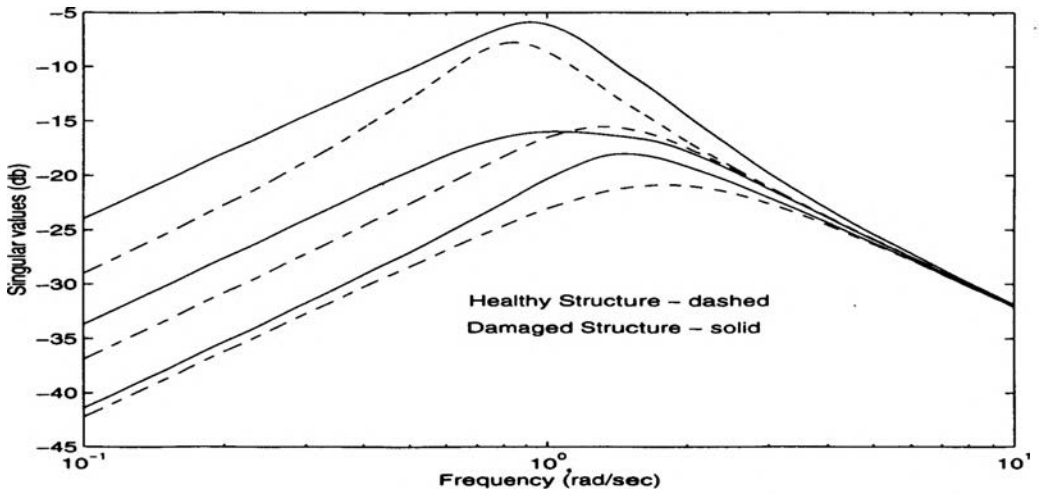

Figure 10. Difference in singular values under damage scenario 1

Modeling the three-bar truss structure in Figure 9 using FEM, the lumped mass matrix M, stiffness matrix K and damping matrix D are determine to be

$$M = \begin{bmatrix} 0.5(m_1 + m_2) & 0 & 0 \\ 0 & 0.5(m_1 + m_2) & 0 \\ 0 & 0 & 0.5(m_2 + m_3) \end{bmatrix} \tag{212}$$

$$K = \begin{bmatrix} 0.25(k_1 + k_2) & 0.433(k_1 - k_2) & -0.25k_2 \\ 0.433(k_1 - k_2) & 0.75(k_1 + k_2) & 0.433k_2 \\ -0.25k_2 & 0.433k_2 & 0.25k_{2+k_3} \end{bmatrix} \tag{213}$$

and

$$D = \begin{bmatrix} 0.25(d_1 + d_2) & 0.433(d_1 - d_2) & -0.25d_2 \\ 0.433(d_1 - d_2) & 0.75(d_1 + d_2) & 0.433d_2 \\ -0.25d_2 & 0.433d_2 & 0.25d_2 + d_3 \end{bmatrix}. \tag{214}$$

It has been assumed that a damping parameter which allows to model the damping in the same way the stiffness is modeled, is known for each structural element. Using Equation (93), this model, and the structural parameters provided in Table VIII (damage scenario 1), the respective state space matrices A and A_d for the healthy and damaged structure are determined to be

$$A = \begin{bmatrix} 0 & 0 & 0 & 1 & 0 & 0 \\ 0 & 0 & 0 & 0 & 1 & 0 \\ 0 & 0 & 0 & 0 & 0 & 1 \\ -0.875 & 0 & 0.4375 & -0.75 & 0 & 0.375 \\ 0 & -2.625 & -0.7578 & 0 & -2.25 & -0.6495 \\ 0.4375 & -0.7578 & -2.1875 & 0.375 & -0.6495 & -1.875 \end{bmatrix} \tag{215}$$

and

$$A_d = \begin{bmatrix} 0 & 0 & 0 & 1 & 0 & 0 \\ 0 & 0 & 0 & 0 & 1 & 0 \\ 0 & 0 & 0 & 0 & 0 & 1 \\ -0.5906 & 0.4926 & 0.4375 & 0.4688 & -0.4871 & 0.0938 \\ 0.4926 & -1.7719 & -0.7578 & -0.4871 & -1.4062 & -0.1624 \\ 0.4375 & -0.7578 & -2.1875 & 0.0938 & -0.1624 & -1.5938 \end{bmatrix}. \tag{216}$$

Given that the structural mass does not change with damage, the state space matrix B is the same for both healthy and damaged structure, i.e.,

$$B = B_d = \begin{bmatrix} 0 & 0 & 0 \\ 0 & 0 & 0 \\ 0 & 0 & 0 \\ 0.25 & 0 & 0 \\ 0 & 0.25 & 0 \\ 0 & 0 & 0.25 \end{bmatrix}. \tag{217}$$

The eigenvalues of matrices A and A_d are respectively described in Tables IX and X.

Table IX: Eigenvalues of matrix A, three-bar 3-DOF

Eigenvalues	Damping	Freq. (rad/sec)
$-0.305 \pm j0.787$	0.362	0.844
$-0.75 \pm j1.090$	0.567	1.323
$-1.382 \pm j1.147$	0.770	1.760

Table X: Eigenvalues of matrix A_d, three-bar 3-DOF

Eigenvalues	Damping	Freq. (rad/sec)
$-0.354 \pm j0.896$	0.368	0.964
$-0.649 \pm j0.416$	0.842	0.771
$-0.731 \pm j1.419$	0.458	1.60

Both healthy and damaged structures were simulated to get input-output data. The simulations were performed using the physical coordinate state space representation. The velocity of each DOF was measured as the structural response. Only one DOF was excited at a time with a random signal. The sampling time used in simulation was chosen considering the fastest eigenvalue of the structures; they were choose to be slightly over 5 times faster. The sampling time in the simulation of the healthy structure was $T_s = 0.5598 sec$, and $T_s = 0.6298 sec$ for the damaged structure. The state space representation of the structures were estimated using the two mentioned system identification procedures. The system identification procedures were used to determine 9 single-input single-output (SISO) systems, which were combined and reduced to a 6^{th} order state space representation.

The ERA algorithm was used to estimate the damaged structure state space representation from the estimated MPs. The MPs were estimated using a feedforward neural network. In order to perform the structural diagnosis it was assumed that the model for the healthy structure was known.

A feedforward neural network with 90 neurons at the input layer, 170 neurons at the hidden layer and 1 neuron at the output layer was found to learn the structural input-output relationship with an RMS error in the order of 10^{-4}. Once the network was trained for each SISO system, the weights were used to estimate the Markov parameters of the system, which then were used by the ERA to estimate the state space representation of the structure, as explained in Section III. The information required to perform the linear transformation into the physical coordinates of the

structure, as well as the structural diagnosis, is contained in the state space pair matrices $\left\{A_{d_{id}}, B_{d_{id}}\right\}$, which for the damage scenario 1 were estimated to be

$$A_{d_{id}} = \begin{bmatrix} -0.4665 & 0.9084 & -0.2730 & 0.1004 & -0.1112 & -0.0079 \\ -0.9086 & -0.0131 & 0.0136 & -0.2182 & 0.0044 & 0.0771 \\ 0.2734 & 0.0134 & -0.0468 & 0.9451 & -0.0242 & -0.4684 \\ 0.0100 & 0.2181 & -0.9438 & -1.4473 & -0.0202 & 0.0248 \\ 0.1118 & 0.0027 & -0.0188 & 0.0283 & -0.0110 & -1.4593 \\ -0.0096 & -0.0771 & 0.4670 & 0.0192 & 1.4455 & -1.5227 \end{bmatrix} \tag{218}$$

and

$$B_{d_{id}} = \begin{bmatrix} -0.4655 & 0.1735 & -0.1192 \\ -0.0464 & -0.0623 & -0.0299 \\ 0.0905 & -0.0068 & 0.0390 \\ 0.1885 & 0.4745 & -0.0143 \\ 0.0378 & -0.0165 & 0.0120 \\ 0.0954 & -0.0606 & -0.4888 \end{bmatrix}. \tag{219}$$

The difference in the singular values between the identified damaged structure versus the nominal damaged structure is shown in Figure 11. The suggested procedure to transform the arbitrary identified damaged structure into the physical coordinates was used. The procedure involve in the linear transformation process is provided in the Appendix A.

From the identified state space representation already transformed into the physical coordinate, the matrices K_d and D_d are determined to be

$$K_d = \begin{bmatrix} 2.3669 & -2.0280 & -1.8058 \\ -1.9455 & 7.1459 & 3.0160 \\ -1.7547 & 3.1015 & 8.7988 \end{bmatrix} \tag{220}$$

and

$$D_d = \begin{bmatrix} 1.8725 & 1.9969 & -0.3651 \\ 1.9789 & 5.7614 & 0.6997 \\ -0.3415 & 0.6728 & 6.3954 \end{bmatrix}. \tag{221}$$

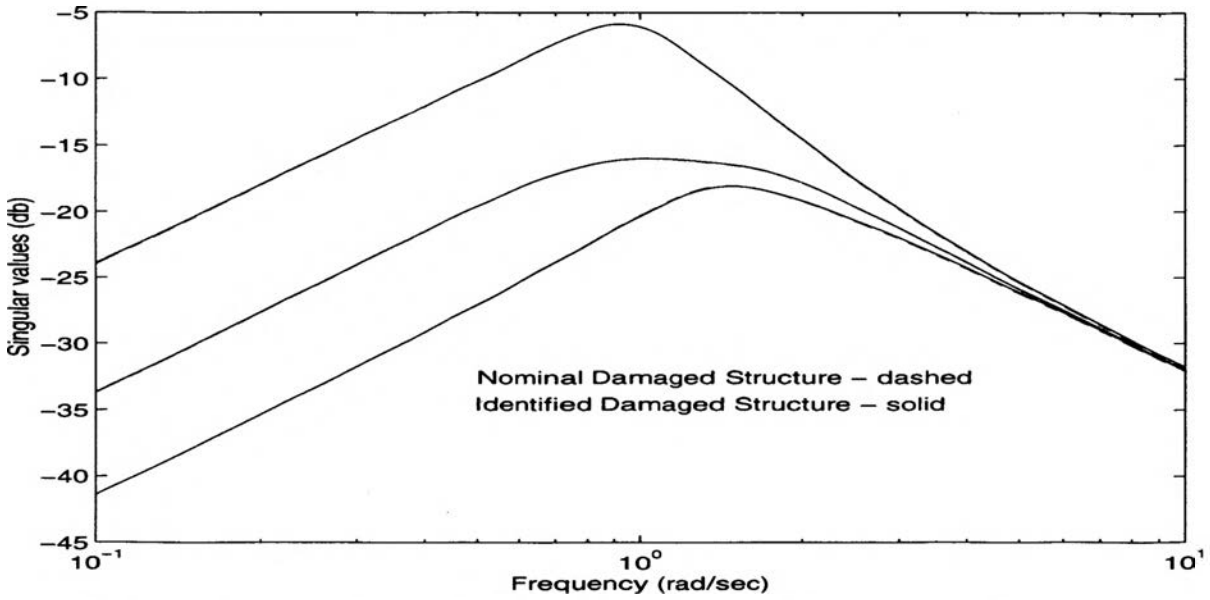

Figure 11. Difference in singular values between nominal and identified damaged structure using ERA for system identification

Using Equations (106) and (108), the equations for determining the damping and stiffness reduction factors, a_i and b_i respectively, are determined to be

$$\begin{bmatrix} 1.5 & 1.5 & 0 \\ 2.5981 & -2.5981 & 0 \\ 0 & -1.5 & 0 \\ 2.5981 & -2.5981 & 0 \\ 4.5 & 4.5 & 0 \\ 0 & 2.5981 & 0 \\ 0 & -1.5 & 0 \\ 0 & 2.5981 & 0 \\ 0 & 1.5 & 6 \end{bmatrix} \begin{bmatrix} a_1 \\ a_2 \\ a_3 \end{bmatrix} = \begin{bmatrix} -1.1275 \\ 1.9969 \\ 1.1349 \\ 1.9789 \\ -3.2386 \\ -1.8984 \\ 1.1585 \\ -1.9253 \\ -1.1046 \end{bmatrix} \tag{222}$$

and

$$\begin{bmatrix} 1.75 & 1.75 & 0 \\ 3.0311 & -3.0311 & 0 \\ 0 & -1.75 & 0 \\ 3.0311 & -3.0311 & 0 \\ 5.25 & 5.25 & 0 \\ 0 & 3.0311 & 0 \\ 0 & -1.75 & 0 \\ 0 & 3.0311 & 0 \\ 0 & 1.75 & 7 \end{bmatrix} \begin{bmatrix} b_1 \\ b_2 \\ b_3 \end{bmatrix} = \begin{bmatrix} -1.331 \\ -2.0280 \\ -0.0558 \\ -1.9455 \\ -3.3541 \\ -0.0151 \\ -0.0047 \\ 0.0704 \\ 0.0488 \end{bmatrix}. \tag{223}$$

Solving Equations (222) and (223), the following results are obtained

$$\begin{bmatrix} a_1 \\ a_2 \\ a_3 \end{bmatrix} = \begin{bmatrix} 0.0210 \\ -0.7437 \\ 0.0018 \end{bmatrix} \tag{224}$$

and

$$\begin{bmatrix} b_1 \\ b_2 \\ b_3 \end{bmatrix} = \begin{bmatrix} -0.6479 \\ 0.0090 \\ 0.0047 \end{bmatrix}. \tag{225}$$

From these results it can be seen that the 75% reduction on the damping parameter for the structural element #2 is estimated to be a reduction of 74.37%, while the 65% reduction on the stiffness parameter for the structural element #1 is estimated to be a reduction of 64.79%. Considering that the system identification procedure introduces uncertainty into the damage detection, the other estimated reduction factors may be disregarded.

Considering the same damage scenario 1, as shown in Table VIII, the proposed GDDA was repeated using the *MATLAB System Identification Toolbox* for identification purpose. Once the obtained arbitrary state space representation was transformed into the structural physical coordinates the following matrix $A_{d_{ph}}$ was obtained

$$A_{d_{ph}} = \begin{bmatrix} 0 & 0 & 0 & 1 & 0 & 0 \\ 0 & 0 & 0 & 0 & 1 & 0 \\ 0 & 0 & 0 & 0 & 0 & 1 \\ -0.5990 & 0.4760 & 0.4333 & -0.4468 & -0.4591 & 0.0840 \\ 0.5166 & -1.7452 & -0.7670 & -0.4574 & -1.3373 & -0.1563 \\ 0.4528 & -0.7495 & -2.1967 & 0.0858 & -0.1591 & -1.5620 \end{bmatrix}. \tag{226}$$

Figure 12 shows the difference between the singular values for the identified-damaged structure versus the nominal damaged structure.

From the matrix A, as shown in Equation (226), the matrices K_d and D_d are determined to be

$$K_d = \begin{bmatrix} 2.3959 & -1.9040 & -1.7333 \\ -2.0666 & 6.9809 & 3.0679 \\ -1.8112 & 2.9980 & 8.7869 \end{bmatrix} \tag{227}$$

and

$$D_d = \begin{bmatrix} 1.7872 & 1.8366 & -0.3359 \\ 1.8296 & 5.3494 & 0.6252 \\ -0.3432 & 0.6364 & 6.2480 \end{bmatrix}. \tag{228}$$

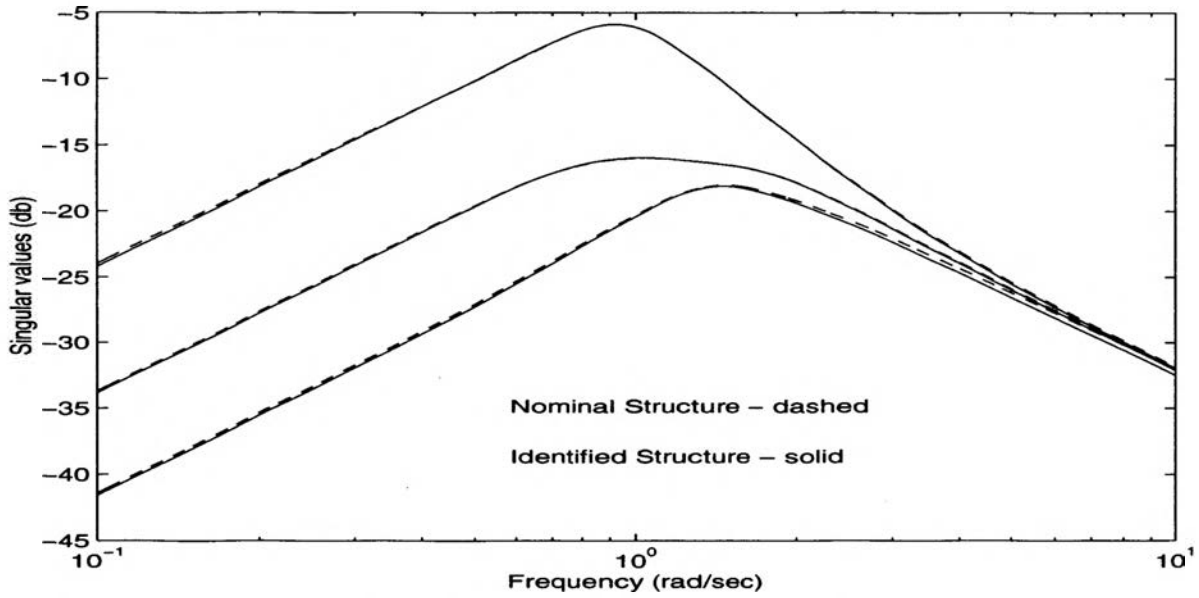

Figure 12. Difference in singular values, nominal structure versus identified

Using Equations (106) and (108), the following equations for determining the damping and stiffness reduction factors, a_i and b_i respectively, are determined to be

$$\begin{bmatrix} 1.5 & 1.5 & 0 \\ 2.5981 & -2.5981 & 0 \\ 0 & -1.5 & 0 \\ 2.5981 & -2.5981 & 0 \\ 4.5 & 4.5 & 0 \\ 0 & 2.5981 & 0 \\ 0 & -1.5 & 0 \\ 0 & 2.5981 & 0 \\ 0 & 1.5 & 6 \end{bmatrix} \begin{bmatrix} a_1 \\ a_2 \\ a_3 \end{bmatrix} = \begin{bmatrix} -1.2128 \\ 1.8366 \\ 1.1641 \\ 1.8296 \\ -3.6506 \\ -1.9729 \\ 1.1568 \\ -1.9617 \\ -1.2520 \end{bmatrix} \tag{229}$$

and

$$\begin{bmatrix} 1.75 & 1.75 & 0 \\ 3.0311 & -3.0311 & 0 \\ 0 & -1.75 & 0 \\ 3.0311 & -3.0311 & 0 \\ 5.25 & 5.25 & 0 \\ 0 & 3.0311 & 0 \\ 0 & -1.75 & 0 \\ 0 & 3.0311 & 0 \\ 0 & 1.75 & 7 \end{bmatrix} \begin{bmatrix} b_1 \\ b_2 \\ b_3 \end{bmatrix} = \begin{bmatrix} -1.1041 \\ -1.9040 \\ 0.0167 \\ -2.0666 \\ -3.5191 \\ 0.0368 \\ -0.0612 \\ -0.0331 \\ 0.0369 \end{bmatrix}. \tag{230}$$

Solving Equations (229) and (230)

$$\begin{bmatrix} a_1 \\ a_2 \\ a_3 \end{bmatrix} = \begin{bmatrix} -0.0524 \\ -0.7593 \\ -0.0188 \end{bmatrix} \tag{231}$$

and

$$\begin{bmatrix} b_1 \\ b_2 \\ b_3 \end{bmatrix} = \begin{bmatrix} -0.6615 \\ -0.0024 \\ 0.0059 \end{bmatrix}. \tag{232}$$

From these results, it can be seen that the 75% reduction in the damping parameter for structural element #2 is estimated to be 75.93% reduction, while the 65% reduction of the stiffness parameter for the structural element #1 is estimated to be a reduction of 66.15%. The other estimated reduction factors may be disregarded because the uncertainty introduced by the system identification procedure.

The proposed GDDA was applied for the damage scenarios 2, 3 and 4 as described in Table VIII; and the system identification was performed using the *MATLAB System Identification Toolbox*. The obtained results are summarized in Tables XI, XII and XIII.

Table XI: Obtained results on damage scenario 2

Reduction Factor	Nominal Reduction (%)	Estimated Reduction (%)
a_1	30	34.06
a_2	0	15.30
a_3	0	11.41
b_1	0	0.38
b_2	45	45.87
b_3	0	0.37

Table XII: Obtained results on damage scenario 3

Reduction Factor	Nominal Reduction (%)	Estimated Reduction (%)
a_1	0	2.9
a_2	0	7.91
a_3	37.5	40.22
b_1	0	0.43
b_2	0	0.39
b_3	55	55.02

Table XIII: Obtained results on damage scenario 4

Reduction Factor	Nominal Reduction (%)	Estimated Reduction (%)
a_1	30	33.69
a_2	75	75.83
a_3	37.5	38.28
b_1	65	65.59
b_2	45	45.06
b_3	55	54.90

Considering the uncertainty added by the system identification any reduction factor which is much less than an estimated reduction factor may be disregarded. From the obtained results, it can be seen that the reduction in stiffness was always properly identified, while the reduction in damping had a case, damage scenario 2, in which two undamaged structural elements where classified as damaged elements. In this case, only the damping parameter for the structural element number 1 was varied, and it was estimated to be of 34.06%; even when the damping parameter for the other two elements were not varied, the procedure reflected a reduction factor of 15.30% and 11.41% for the structural elements 2 and 3, respectively. Note that the damage scenario 2 was included in damage scenario 4; when the damage scenario 4 was considered all damage extents were properly identified.

The errors obtained in estimating the damping reduction were in general, larger that the errors obtained in estimating the stiffness reductions, which indicates that the damping effect is more difficult to identify than the stiffness effect.

VI. CONCLUSIONS AND FUTURE WORK

A global damage detection algorithm (GDDA) for bridge-like structures has been proposed. This algorithm assumes the mass of the structural element does not change when it is damaged, which is a reasonable assumptions for bridge-like structures. The proposed algorithm provides for determining which structural elements had undergone a reduction in the stiffness and/or damping parameters; additionally, it determines the extension of the damage by estimating the reduction factor for each stiffness and damping parameter.

A finite element model (FEM) of a test structure has been provided. The natural frequencies computed from the obtained FEM do not match the obtained experimental natural frequencies. A more accurate FEM should be obtained in order to use it for damage detection purpose.

The proposed GDDA is based on the state space representation of the structure in the physical coordinates. The estimated state space representation for the structure using any system identification will correspond to an arbitrary set of states, but in order to apply the proposed GDDA the state space representation must correspond to the physical coordinate. The need arises for a linear transformation to transform the identified arbitrary state space representation into the physical coordinate. A method to perform this linear transformation has been proposed. The proposed procedure for linearly transform any arbitrary state space representation into the physical coordinate imposes the limitation that the number of actuators on the structure must be equal to the number of degrees-of-freedom (DOF). How to overcome the

limitation imposed by the proposed linear transformation should be further investigated.

The proposed GDDA has been successfully applied on a 3-DOF mass-damper-spring system as well as on a simulated three-bar-truss structure with 3-DOF. The obtained results indicate the proposed GDDA constitutes a valuable method for the damage detection in bridge-like structures. Considering that the proposed GDDA is based on time domain data, it provides for real time damage detection.

APPENDIX A

EXAMPLE OF LINEAR TRANSFORMATION PROCEDURE

The proposed procedure to obtain the linear transformation into the physical coordinate will be shown step-by-step for a numerical example, which corresponds to the three-bar 3-DOF structure considered in chapter V under the damage scenario #1. Consider the following identified matrices for the damaged structure:

$$A_{d_{id}} = \begin{bmatrix} -0.4665 & 0.9084 & -0.2730 & 0.1004 & -0.1112 & -0.0079 \\ -0.9086 & -0.0131 & 0.0136 & -0.2182 & 0.0044 & 0.0771 \\ 0.2734 & 0.0134 & -0.0468 & 0.9451 & -0.0242 & -0.4684 \\ 0.0100 & 0.2181 & -0.9438 & -1.4473 & -0.0202 & 0.0248 \\ 0.1118 & 0.0027 & -0.0188 & 0.0283 & -0.0110 & -1.4593 \\ -0.0096 & -0.0771 & 0.4670 & 0.0192 & 1.4455 & -1.5227 \end{bmatrix} \tag{A3}$$

and

$$B_{d_{id}} = \begin{bmatrix} -0.4655 & 0.1735 & -0.1192 \\ -0.0464 & -0.0623 & -0.0299 \\ 0.0905 & -0.0068 & 0.0390 \\ 0.1885 & 0.4745 & -0.0143 \\ 0.0378 & -0.0165 & 0.0120 \\ 0.0954 & -0.0606 & -0.4888 \end{bmatrix}. \tag{A4}$$

Equations (A1) and (A2) can be expressed as

$$A_{d_{id}} = \begin{bmatrix} A_{d_{id_{\hat{1}}}} & A_{d_{id_{\hat{2}}}} & A_{d_{id_{\hat{3}}}} & A_{d_{id_{\hat{4}}}} & A_{d_{id_{\hat{5}}}} & A_{d_{id_{\hat{6}}}} \end{bmatrix} = \begin{bmatrix} A_{d_{id_{\rightarrow 1}}} \\ A_{d_{id_{\rightarrow 2}}} \\ A_{d_{id_{\rightarrow 3}}} \\ A_{d_{id_{\rightarrow 4}}} \\ A_{d_{id_{\rightarrow 5}}} \\ A_{d_{id_{\rightarrow 6}}} \end{bmatrix} \tag{A5}$$

and

$$B_{d_{id}} = \begin{bmatrix} B_{d_{id_{\rightarrow 1}}} & B_{d_{id_{\rightarrow 2}}} & B_{d_{id_{\rightarrow 3}}} & B_{d_{id_{\rightarrow 4}}} & B_{d_{id_{\rightarrow 5}}} & B_{d_{id_{\rightarrow 6}}} \end{bmatrix}^T . \tag{A6}$$

The mass matrix for the structure is

$$M = \begin{bmatrix} 4 & 0 & 0 \\ 0 & 4 & 0 \\ 0 & 0 & 4 \end{bmatrix} . \tag{A7}$$

Using equation (184) the following set equation are obtained:

$$\begin{bmatrix} t_{(1,4)} \\ t_{(1,5)} \\ t_{(1,6)} \end{bmatrix} = M^T \begin{bmatrix} -0.4655 \\ 0.1735 \\ -0.1192 \end{bmatrix} = \begin{bmatrix} -1.8618 \\ 0.6939 \\ -0.4768 \end{bmatrix} , \tag{A8}$$

$$\begin{bmatrix} t_{(2,4)} \\ t_{(2,5)} \\ t_{(2,6)} \end{bmatrix} = M^T \begin{bmatrix} -0.0464 \\ -0.0623 \\ -0.0299 \end{bmatrix} = \begin{bmatrix} -0.1857 \\ -0.2493 \\ -0.1197 \end{bmatrix} , \tag{A9}$$

$$\begin{bmatrix} t_{(3,4)} \\ t_{(3,5)} \\ t_{(3,6)} \end{bmatrix} = M^T \begin{bmatrix} 0.0905 \\ -0.0068 \\ 0.0390 \end{bmatrix} = \begin{bmatrix} 0.3622 \\ -0.0271 \\ 0.1561 \end{bmatrix}, \tag{A10}$$

$$\begin{bmatrix} t_{(4,4)} \\ t_{(4,5)} \\ t_{(4,6)} \end{bmatrix} = M^T \begin{bmatrix} 0.1885 \\ 0.4745 \\ -0.0143 \end{bmatrix} = \begin{bmatrix} 0.7541 \\ 1.8980 \\ -0.0572 \end{bmatrix}, \tag{A11}$$

$$\begin{bmatrix} t_{(5,4)} \\ t_{(5,5)} \\ t_{(5,6)} \end{bmatrix} = M^T \begin{bmatrix} 0.0378 \\ -0.0165 \\ 0.0120 \end{bmatrix} = \begin{bmatrix} 0.1514 \\ -0.0658 \\ 0.0478 \end{bmatrix} \tag{A12}$$

and

$$\begin{bmatrix} t_{(6,4)} \\ t_{(6,5)} \\ t_{(6,6)} \end{bmatrix} = M^T \begin{bmatrix} 0.0954 \\ -0.0606 \\ -0.4888 \end{bmatrix} = \begin{bmatrix} 0.3817 \\ -0.2424 \\ -1.9550 \end{bmatrix}. \tag{A13}$$

From equations (A4) to (A9) it is obtained that

$$\begin{bmatrix} T_{\hat{4}} & T_{\hat{5}} & T_{\hat{6}} \end{bmatrix} = \begin{bmatrix} -1.8618 & 0.6939 & -0.4768 \\ -0.1857 & -0.2493 & -0.1197 \\ 0.3622 & -0.0271 & 0.1561 \\ 0.7541 & 1.8980 & -0.0572 \\ 0.1514 & -0.0658 & 0.0478 \\ 0.3817 & -0.2424 & -1.9550 \end{bmatrix}. \tag{A14}$$

The first 3 columns of the transformation matrix T remain to be determined; for this purpose equation (188) will be used, where the partitioned matrices P_{11}, P_{12} and P_{22} are respectively given by equations (192), (193) and (194), so that

$$P_{11} = \begin{bmatrix} P_{11_1} & P_{11_2} \end{bmatrix} \tag{A15}$$

where

$$P_{11_1} = \begin{bmatrix} A_{id_{\hat{1}}} & 0_{6,2} & A_{id_{\hat{2}}} & 0_{6,2} & A_{id_{\hat{3}}} & 0_{6,1} & 0_{6,1} \\ 0_{6,1} & A_{id_{\hat{1}}} & 0_{6,2} & A_{id_{\hat{2}}} & 0_{6,2} & A_{id_{\hat{3}}} & 0_{6,1} \\ 0_{6,1} & 0_{6,1} & A_{id_{\hat{1}}} & 0_{6,2} & A_{id_{\hat{2}}} & 0_{6,2} & A_{id_{\hat{3}}} \end{bmatrix} \tag{A16}$$

and

$$P_{11_2} = \begin{bmatrix} A_{id_{\hat{4}}} & 0_{6,2} & A_{id_{\hat{5}}} & 0_{6,2} & A_{id_{\hat{6}}} & 0_{6,1} & 0_{6,1} \\ 0_{6,1} & A_{id_{\hat{4}}} & 0_{6,2} & A_{id_{\hat{5}}} & 0_{6,2} & A_{id_{\hat{6}}} & 0_{6,1} \\ 0_{6,1} & 0_{6,1} & A_{id_{\hat{4}}} & 0_{6,2} & A_{id_{\hat{5}}} & 0_{6,2} & A_{id_{\hat{6}}} \end{bmatrix} \tag{A17}$$

$$P_{12} = \begin{bmatrix} -T_{\hat{4}} & 0_{6,5} & -T_{\hat{5}} & 0_{6,5} & -T_{\hat{6}} & 0_{6,4} & 0_{6,1} \\ 0_{6,1} & -T_{\hat{4}} & 0_{6,5} & -T_{\hat{5}} & 0_{6,5} & -T_{\hat{6}} & 0_{6,4} \\ 0_{6,2} & -T_{\hat{4}} & 0_{6,5} & -T_{\hat{5}} & 0_{6,5} & -T_{\hat{6}} & 0_{6,3} \end{bmatrix} \tag{A18}$$

and

$$P_{22} = \begin{bmatrix} 0_{3,3} & t_{14}I_3 & 0_{3,3} & t_{15}I_3 & 0_{3,3} & t_{16}I_3 \\ 0_{3,3} & t_{24}I_3 & 0_{3,3} & t_{25}I_3 & 0_{3,3} & t_{26}I_3 \\ 0_{3,3} & t_{34}I_3 & 0_{3,3} & t_{35}I_3 & 0_{3,3} & t_{36}I_3 \\ 0_{3,3} & t_{44}I_3 & 0_{3,3} & t_{45}I_3 & 0_{3,3} & t_{46}I_3 \\ 0_{3,3} & t_{54}I_3 & 0_{3,3} & t_{55}I_3 & 0_{3,3} & t_{56}I_3 \\ 0_{3,3} & t_{64}I_3 & 0_{3,3} & t_{65}I_3 & 0_{3,3} & t_{66}I_3 \end{bmatrix}; \tag{A19}$$

and v_3 is

$$v_3 = \begin{bmatrix} {}^{A}_{1}T_{\hat{4}} \\ {}^{A}_{1}T_{\hat{5}} \\ {}^{A}_{1}T_{\hat{6}} \\ {}^{A}_{2}T_{\hat{4}} \\ {}^{A}_{2}T_{\hat{5}} \\ {}^{A}_{2}T_{\hat{6}} \\ {}^{A}_{3}T_{\hat{4}} \\ {}^{A}_{3}T_{\hat{5}} \\ {}^{A}_{3}T_{\hat{6}} \\ {}^{A}_{4}T_{\hat{4}} \\ {}^{A}_{4}T_{\hat{5}} \\ {}^{A}_{4}T_{\hat{6}} \\ {}^{A}_{5}T_{\hat{4}} \\ {}^{A}_{5}T_{\hat{5}} \\ {}^{A}_{5}T_{\hat{6}} \\ {}^{A}_{6}T_{\hat{4}} \\ {}^{A}_{6}T_{\hat{5}} \\ {}^{A}_{6}T_{\hat{6}} \end{bmatrix} = \begin{bmatrix} 0.5889 \\ -0.5138 \\ 0.0807 \\ 1.5645 \\ -1.0606 \\ 0.2989 \\ 0.0018 \\ 2.0966 \\ 0.7214 \\ -1.4858 \\ -2.7736 \\ -0.1450 \\ -0.7528 \\ 0.4854 \\ 2.7943 \\ -0.1466 \\ 0.3102 \\ 3.1316 \end{bmatrix}. \tag{A20}$$

From equation (188) v_1 can be determined,

$$v_1 = \begin{bmatrix} t_{11} \\ t_{12} \\ t_{13} \\ t_{21} \\ t_{22} \\ t_{23} \\ t_{31} \\ t_{32} \\ t_{33} \\ t_{41} \\ t_{42} \\ t_{43} \\ t_{51} \\ t_{52} \\ t_{53} \\ t_{61} \\ t_{62} \\ t_{63} \end{bmatrix} = -P_{11}^{-1}P_{12}(P_{22} - P_{11}^{-1}P_{12})^{-1}v_3 = \begin{bmatrix} 0.1013 \\ -0.5240 \\ -0.3904 \\ 1.3644 \\ -1.5325 \\ 0.0808 \\ 0.1447 \\ 2.2647 \\ 0.9332 \\ -0.1889 \\ 0.3271 \\ 0.0268 \\ -0.7186 \\ 0.4743 \\ 2.8454 \\ 0.0791 \\ -0.1772 \\ -0.0714 \end{bmatrix}. \tag{A21}$$

Therefore, the transformation matrix has been determined to be

$$T = \begin{bmatrix} 0.1013 & -0.5240 & -0.3904 & -1.8618 & 0.6939 & -0.4768 \\ 1.3644 & -1.5325 & 0.0808 & -0.1857 & -0.2493 & -0.1197 \\ 0.1447 & 2.2647 & 0.9332 & 0.3622 & 0.0271 & 0.1561 \\ -0.1889 & 0.3271 & 0.0268 & 0.7541 & 1.8980 & -0.0572 \\ -0.7186 & 0.4743 & 2.8454 & 0.1514 & -0.0658 & 0.0478 \\ 0.0791 & -0.1772 & -0.0714 & 0.3817 & -0.2424 & -1.9550 \end{bmatrix}. \tag{A22}$$

Now, the transformation matrix T is known; therefore, the physical coordinate state space

matrix $A_{d_{ph}}$ can be determined using equation (115),

$$A_{d_{ph}} = T^{-1} A_{d_{id}} T = \begin{bmatrix} 0 & 0 & 0 & 1 & 0 & 0 \\ 0 & 0 & 0 & 0 & 1 & 0 \\ 0 & 0 & 0 & 0 & 0 & 1 \\ -0.5917 & 0.5070 & 0.4515 & -0.4681 & -0.4992 & 0.0913 \\ 0.4864 & -1.7865 & -0.7540 & 0.4947 & -1.4403 & -0.1749 \\ 0.4387 & -0.7754 & -2.1997 & 0.0854 & -0.1682 & -1.5989 \end{bmatrix}. \quad \text{(A23)}$$

APPENDIX B

SWEPT SINE FREQUENCY RESPONSES

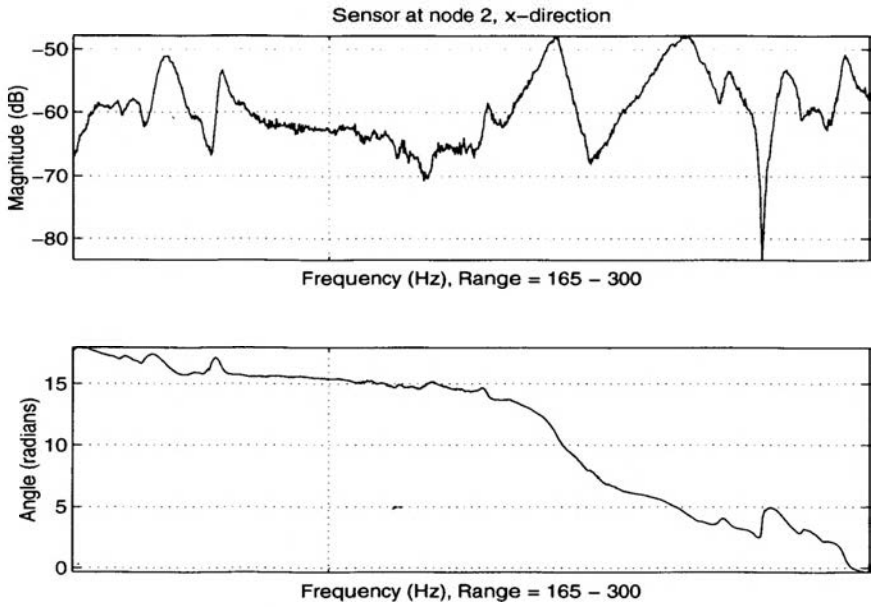

Figure 13. Swept sine frequency response, sensor at node 2, *X*-direction

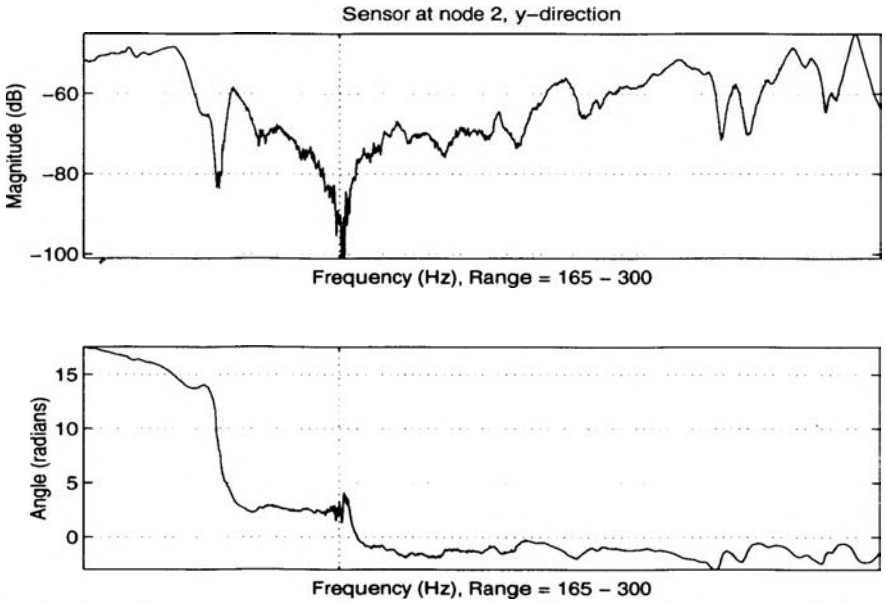

Figure 14. Swept sine frequency response, sensor at node 2, *Y*-direction

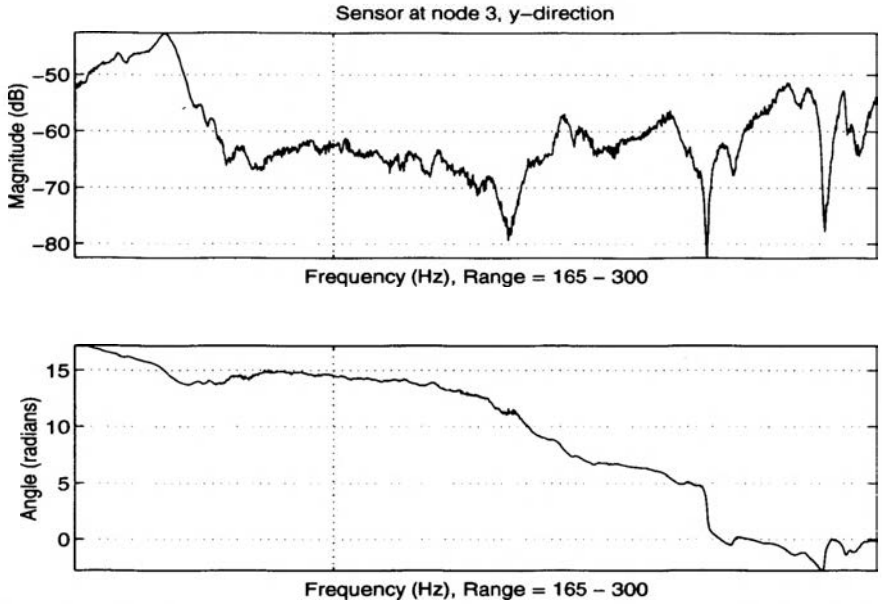

Figure 15. Swept sine frequency response, sensor at node 3, *Y*-direction

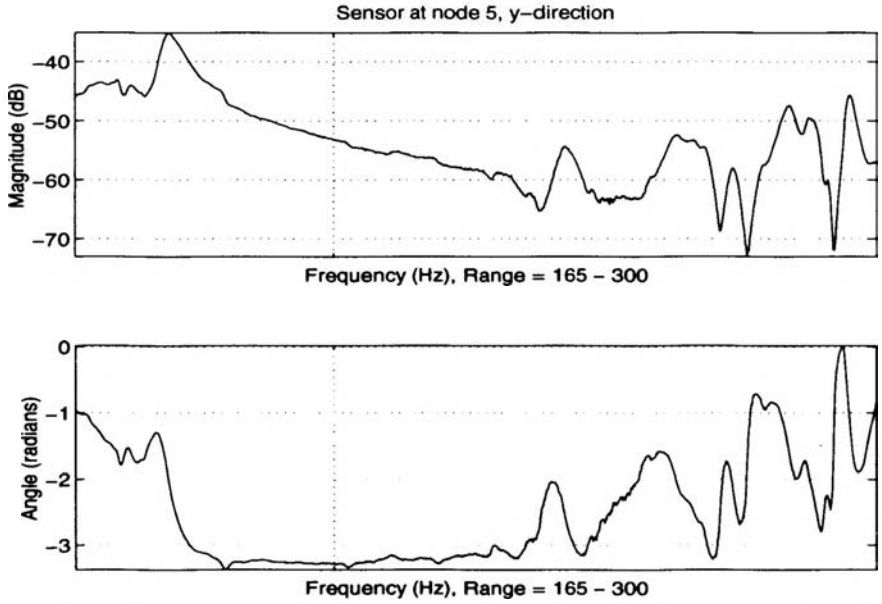

Figure 16. Swept sine frequency response, sensor at node 5, *Y*-direction

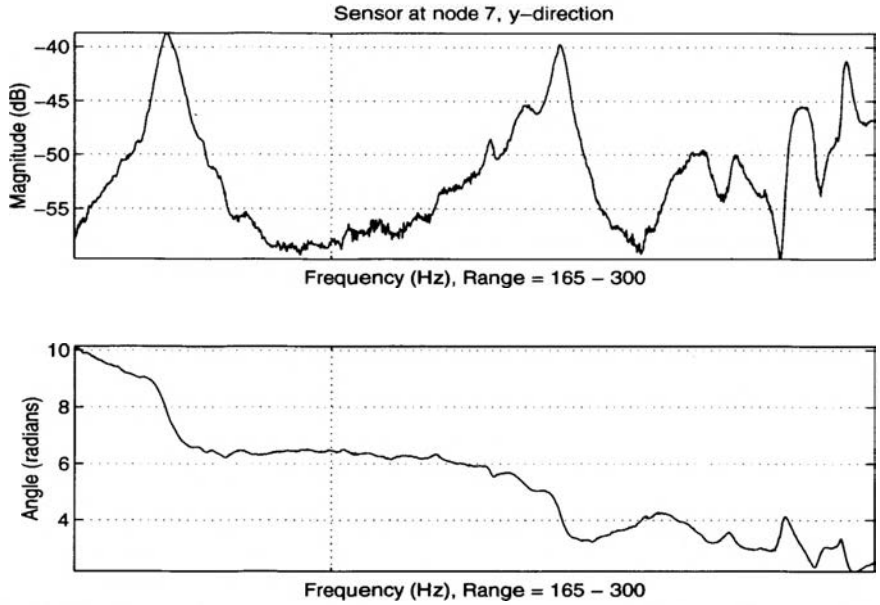

Figure 17. Swept sine frequency response, sensor at node 7, *Y*-direction

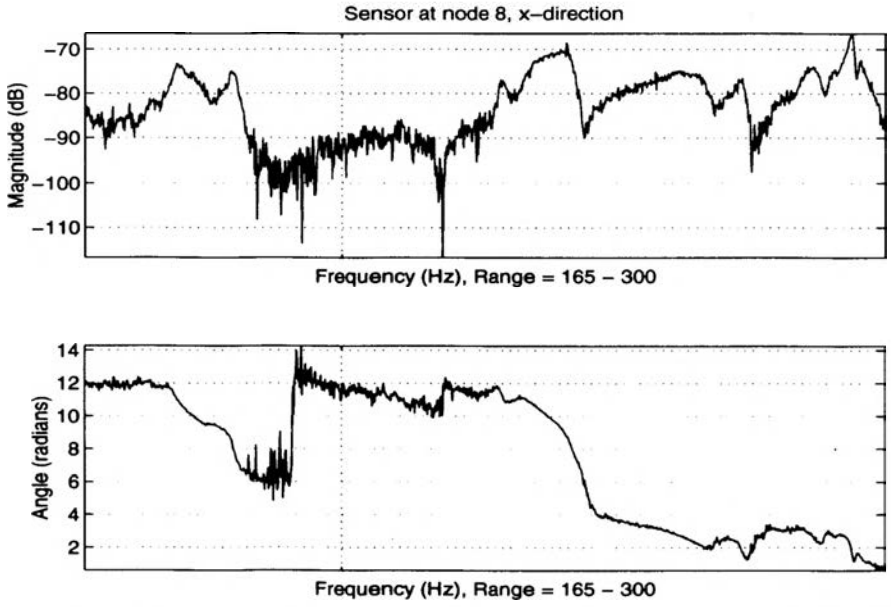

Figure 18. Swept Sine frequency response, sensor at node 8, X-direction

BIBLIOGRAPHY

1. Chen, J.C. and J.A. Garba, "On-Orbit Damage Assessment for Large Space Structures", *AIAA Journal* Vol. 26, No. 9, pp. 1119-1126, 1988.

2. Lim, T.W. and T.A.L. Kashangaki, "Structural Damage Detection of Space Truss Structures Using Best Achievable Eigenvectors", *AIAA Journal* Vol. 32, No. 5, pp. 1049-1057, 1994.

3. Smith, S.W. and P.E. McGowan, "Locating Damage in a Truss Using Modal Tests", to appear in AIAA Journal of Guidance Control and Dynamics.

4. Smith, S.W. and S.L. Hendricks, "Damage Detection and Location in Large Space Trusses", *Proceedings of the AIAA SDM Issues of the International Space Station*, Williamsburg, Virginia, April 21-22, 1988, pp. 56-63.

5. Smith, S.W., J.R. Baker, M. Kaouk and D.C. Zimmerman, "Mode Shape Expansion for Visualization and Correlation", *Proceedings of the Ninth VPI&SU Symposium on Dynamics and Control of Large Structures*, Blacksburg, Virginia, May 10-12, 1993, pp.385-396.

6. Barai, S.V. and P.C. Pandey, "Vibration Signature Analysis Using Artificial Neural Networks", Journal of Computing in Civil Engineering Vol. 9, No. 4, pp. 259-265, 1995.

7. Manning, R., "Damage Detection in Adaptive Structures Using Neural Networks", *Proc. of the 35th AIAA/ASME/ASCE/AHS/ASC Structures, Structural Dynamics, ans Materials Conferences*, pp. 160-172, 1994.

8. Tsou, P. and M.-H.H. Shen, "Structural Damage Detection and Identification Using Neural Networks", *AIAA Journal* Vol. 32, No. 1, pp. 176-183, 1994.

9. Worden, K., A. Ball and G. Tomlinson, "Neural Networks for Fault Location", *Proc. of the 11th International Modal Analysis Conference*, pp. 47-54, 1993.

10. Wu, X., Ghaboussi and J.H. Garrett, "Use of Neural Networks in Detection of Structural Damage", *Computers and Structures* Vol 42, No. 4, pp. 649-659, 1992.

11. Tang, S.S., K.L. Chen and J.E. Grady, "On the Monitoring of Degradation of Composite Materials Using Pattern Recognition Method", *Proceedings of the American Society of Composites Seventh Technical Conference*, 1992, pp. 716-734.

12. Chaudhry, Z., T. Joseph, F. Sun and C. Rogers, "Local-area health monitoring of aircraft via piezoelectric actuator/sensor patches", *SPIE* Vol. 2443, pp. 268-276, 1995.

13. Inman, D.J. Engineering Vibration. Prentice Hall, 1994.

14. Juang, J.N. and R. S. Pappa, "An Eigensystem Realization Algorithm for Modal Parameter Identification and Model Reduction", *Journal of Guidance, Control and Dynamics* Vol. 8, pp. 620-627, 1985.

15. Damle, R., "Identification and Robust Control of Smart Structures using Neural Networks", Masters Thesis, Department of Electrical Engineering, University of Missouri-Rolla, 1993.

16. Damle, R., V. Rao and F. Kern, "Multivariable Neural Network Based Controllers for Smart Structures", *Journal of Intelligent Material Systems and Structures* Vol. 6, pp. 516-528, 1995.

17. Phan, M., G. H. Lucas, J. N. Juang and R. W. Longman, "Linear System Identification Using Backpropagation Neural Networks", *6th International Conf. on Digital Processing of Signals in Communications, Guidance, Navigation and Control Conf.*, pp. 1180-1194, 1991.

18. Bialasiewicz, J.T., and D. Soloway, "Neural Network Modelling of Dynamical Systems", *Proc. of International Symposium on Intelligent Control,* pp. 500-505, 1990.

VITA

Javier Valentín Sívico was born on August 20, 1972 in Mayagüez, Puerto Rico. He was raised in Aguadilla, Puerto Rico, where he attended the José de Jesús Esteves for his elementary education and the Antolina Vélez Quiñonez Presbyterian Academy for his middle school. He attended the Benito Cerezo Vázquez High School, where he graduated with honors and was awarded the Mathematics Medal.

He received his Bachelor of Science degree in Electrical Engineering from the University of Puerto Rico, Mayagüez Campus (C.A.A.M.) in June 1995, graduating Magna Cum Laude. During his fourth year of undergraduate studies, he was selected by the Johns Hopkins University Applied Physics Laboratory as a GEM fellow. On August 1995, he joined the Master of Science Program of the Electrical Engineering Department at the University of Missouri-Rolla. He is a member of the Eta Kappa Nu, Phi Kappa Phi and Tau Beta Pi.

While attending the University of Missouri-Rolla he has been active at the Society of Hispanic Professional Engineers, where he was the Secretary during the academic year 1996-1997. Also, while attending the University of Missouri-Rolla, he and his wife, Lydia M. Rodríguez Medina, had their first son, Angel Javier Valentín Sívico.

Upon completing the requirements for his Master of Science degree in Electrical Engineering, he will join the E.I. DuPont de Nemours and Company through the DuPont Engineering Field Program.